ACS Energy LETTERS

http://pubs.acs.org/journal/aelccp

FOCUS REVIEW

Hydrogen from Sunlight and Water: A Side-by-Side Comparison between Photoelectrochemical and Solar Thermochemical Water-Splitting

Wen-Hui Cheng,[†] Alberto de la Calle,[†] Harry A. Atwater, Ellen B. Stechel,* and Chengxiang Xiang*

Cite This: *ACS Energy Lett.* 2021, 6, 3096−3113

Read Online

ACCESS | Metrics & More | Article Recommendations | Supporting Information

ABSTRACT: Photoelectrochemical (PEC) and solar thermochemical (STCH) water-splitting represent two promising pathways for direct solar hydrogen generation. PEC water-splitting integrates multiple functional materials and utilizes energetic electrons and holes generated from sunlight to produce hydrogen and oxygen in two half-reactions, while STCH water-splitting couples a series of consecutive chemical reactions and uses absorbed heat from sunlight to generate hydrogen and oxygen in two full reactions. In this Focus Review, the basic operating principles, sunlight utilization, device architecture, reactor design, instantaneous and annually averaged solar-to-hydrogen (STH) conversion efficiency, and the operating conditions and constraints of both pathways are compared. A side-by-side comparison addresses some common sources of confusion and misinterpretation, especially in the evaluation of STH conversion efficiencies, and reveals distinct features and challenges in both PEC and STCH technologies. This Focus Review also addresses materials and device challenges in PEC and STCH for cost-competitive hydrogen generation.

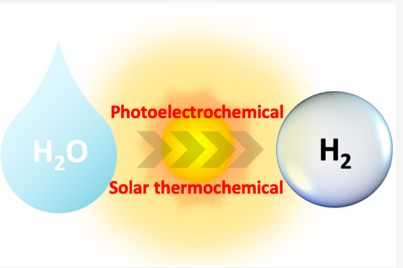

Technologies for large-scale, long-term energy storage that can accommodate weekly and seasonally variable energy needs are expected to play a critical role in a future of significantly expanded renewable energy use. Cost-competitive "green" hydrogen from sunlight could find uses in multiple industrial sectors including transportation, chemical synthesis, iron and steel production, fertilizer synthesis, and in biorefineries. Green hydrogen has the potential to meet long-term, terawatt scale energy storage demands.[1] Water-splitting via solar thermochemical hydrogen (STCH) and photoelectrochemical (PEC) are two important approaches for sunlight-driven "green" hydrogen generation currently being explored by the research and development community. While both technologies use the same feedstock, i.e., sunlight and water, and have a common end product, i.e., hydrogen, the two technologies have rarely been compared and contrasted due to the significant differences in materials, fundamental principles, and operating conditions. Recent DOE-supported benchmarking efforts in the HydroGEN consortium brought multiple technological pathways for advanced water-splitting together to establish and maintain a balanced portfolio of documented "best practices" among four classes of technologies, namely low- and high-temperature electrolysis (LTE and HTE, respectively), PEC, and STCH.[2,3] Recent techno-economic analysis (TEA) of both PEC and STCH water-splitting approaches showed promise for achieving low cost hydrogen using renewable energy inputs. For PEC, various types of PEC devices with forward-looking materials properties and cost estimate yielded levelized cost of H_2 at plant gate at <US$2/kg.[4,5] For STCH, the current estimated H_2 cost is still high (US$4−6/kg),[6] and the solar field and the tower have the highest contribution to this cost. Pathways to achieve a cost target of US$2/kg have been presented in the literature.[7] In this Focus Review, we will first briefly describe the operating principles of the two approaches for direct solar hydrogen generation, PEC and STCH, and their device or reactor embodiment, and then we will compare these two side-by-side in terms of sunlight utilization, anticipated solar-to-hydrogen conversion efficiency, and operating conditions. In addition, we include a discussion of materials and system challenges for each technology. This Focus Review aims to compare the unique aspects and challenges for PEC and STCH, to lay the

Received: April 9, 2021
Accepted: July 22, 2021

https://doi.org/10.1021/acsenergylett.1c00758
ACS Energy Lett. 2021, 6, 3096−3113

groundwork for long-term development of solar fuel technologies. Importantly, we do not aim to make an argument that one approach is better than the other, as both show distinct promise and advantages as well as challenges.

GENERAL OPERATING PRINCIPLES OF PHOTOELECTROCHEMICAL AND SOLAR THERMOCHEMICAL WATER-SPLITTING

Photoelectrochemical (PEC) water-splitting cells are integrated solar fuels generators incorporating multiple functional materials and they couple PEC processes to produce hydrogen and oxygen from sunlight and water. Figure 1a illustrates key

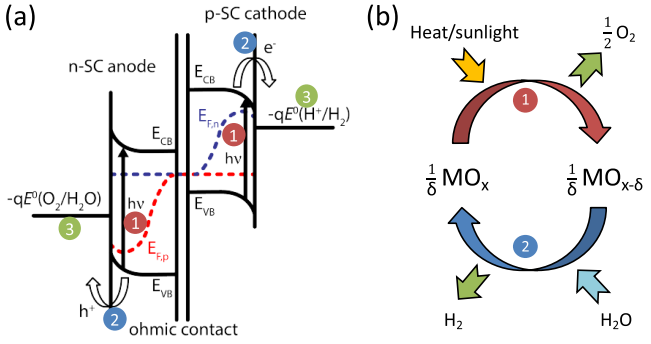

Figure 1. Schematic illustrations of the general operating principles for (a) photoelectrochemical and (b) solar thermochemical advanced water-splitting processes.

photoelectrochemical processes in a typical device in which the semiconductor materials harvest the incident sunlight, and any materials or components in the optical path between the sun and the semiconductors could potentially modulate and alter the light absorption. The light illumination can be from either side of the cell or both sides depending on the detailed configuration of the system. Typically, three main categories include "photocathode and dark anode", "photoanode and dark cathode", and "photocathode and photoanode". In all three categories, the overall voltage generated by the photoabsorbers has to exceed the required voltage for the water-splitting reaction. Figure 1a used "photocathode and photoanode" as the generic illustration for the PEC system. Absorbed photons in the semiconductor material generate energetic electrons and holes, which are transported to electrocatalysts via bulk and interfacial charge transport processes.[8] Next, electrocatalysts perform water-splitting and simultaneously produce gaseous H_2 and O_2 at the catalytic sites. The equations below indicate the possible two half-reactions and corresponding net reaction involved in the complete process:

Half-reaction at cathode (reduction):

$$2H_2O + 2e^- \rightarrow 2OH^- + H_2 \quad (1)$$

Half-reaction at anode (oxidation):

$$2OH^- + 2h^+ \rightarrow \frac{1}{2}O_2 + H_2O \quad (2)$$

$$\text{Net reaction:} \quad H_2O \rightarrow H_2 + \frac{1}{2}O_2 \quad (3)$$

OR

Half-reaction at cathode (reduction):

$$2H^+ + 2e^- \rightarrow H_2 \quad (4)$$

Half-reaction at anode (oxidation):

$$H_2O + 2h^+ \rightarrow \frac{1}{2}O_2 + 2H^+ \quad (5)$$

$$\text{Net reaction:} \quad H_2O \rightarrow H_2 + \frac{1}{2}O_2 \quad (6)$$

In addition, ionic transport between the cathode and anode electrolytes and product separation are necessary to maintain efficient and safe operation of the cell. Note that all these processes couple to produce a single rate of reaction for water-splitting in the PEC device. To overcome the thermodynamic potential (ΔU_{rxn}) between oxygen evolution reaction (OER) at the anode (1.23 V vs RHE, where RHE is the reversible hydrogen electrode potential) and hydrogen evolution reaction (HER) at the cathode (0 V vs RHE), the total voltage (Fermi level splitting) of cathode and anode needs to be large enough to sustain the full reaction.[9] In many cases, as shown in Figure 1, the conduction band edge (E_{CB}) of the cathode and the valence band edge (E_{VB}) of anode straddle the energy levels for water-splitting reactions, e.g., the HER at 0 V vs RHE and the OER at 1.23 V vs RHE.[10,11] It is important to note that band edge positions that straddle the energy levels of water-splitting reactions are not required as long as the overall Fermi-level splitting of the photocathode and photoanode exceeds 1.23 V to sustain the full reaction. In other words, a p-type photocathode with the conduction band position lower than 0 V vs RHE can still drive HER upon illumination due to the surface inversion of the p-type semiconductor that effectively unpinned the band edge position.[12] In addition, solid-state, buried junctions using traditional photovoltaic materials, such as Si, GaAs, etc., are often used to circumvent the stringent requirements for the band edge positions and to achieve high-efficiency solar water-splitting performances.[13−18]

Solar thermochemical (STCH) cycles use sunlight in the form of adsorbed heat to produce hydrogen and oxygen from water. Although water can thermally dissociate just with heat (known as thermolysis), this direct dissociation requires an impractically high operating temperature (>2500 K) to obtain a significant degree (>4%) of hydrogen. Furthermore, the separation of the products at high temperatures is challenging.[19,20] STCH water-splitting reactors circumvent these difficulties by carrying out the dissociation reaction through a series of consecutive chemical reactions, such that O_2 and H_2 are generated in different steps, either separated temporally or spatially.[21] In addition to water as the sole consumed reactant, one or more materials actively participate in the process without being "net" consumed. Many sequences of reactions have been proposed like volatile metal oxide cycles (e.g., Zn/ZnO cycle[22−24] or SnO_2/SnO cycle[25]), phase change stoichiometric oxides (e.g., Fe_3O_4/FeO cycle[26,27] or metal-substituted ferrites cycles[28−30]) or multistep cycles (e.g., hybrid sulfur cycle[31−33] or manganese oxide-based cycle[34−36]). However, currently two-step redox active off-stoichiometric metal oxide (MO_x) thermochemical cycles garner most of the ongoing research efforts among the thermochemical water-splitting cycles,[37] either with cerium-based oxides[38−41] or perovskites.[42−44] The metal oxide cycles involve only two reactions (one per each step) based on a redox swing between

https://doi.org/10.1021/acsenergylett.1c00758
ACS Energy Lett. 2021, 6, 3096−3113

an oxidized and reduced form of a candidate material, MO_x, for which the metal ion (M) can assume multiple oxidation states and the oxygen stoichiometry can vary continuously.[40] eqs 7-9 below summarize the reactions involved in the two-step off-stoichiometric metal oxide cycle:

$$\text{Reduction:} \quad \frac{1}{\delta}MO_x \rightarrow \frac{1}{\delta}MO_{x-\delta} + \frac{1}{2}O_2 \tag{7}$$

$$\text{Oxidation:} \quad \frac{1}{\delta}MO_{x-\delta} + H_2O \rightarrow \frac{1}{\delta}MO_x + H_2 \tag{8}$$

$$\text{Net reaction:} \quad H_2O \rightarrow H_2 + \frac{1}{2}O_2 \tag{9}$$

Figure 1b illustrates the overall operating principle of the two reaction steps in STCH water-splitting. The first step involves the reduction reaction, which is highly endothermic and requires a high-temperature energy source for the reaction to occur. Note that the metal-oxide reduction reaction enthalpy must be higher than the water-splitting reaction enthalpy at the reoxidation temperature, and tends to range between 250 and 500 kJ/mol of H_2.[45] Concentrated solar thermal technologies such as point focus on a solar tower can provide this heat in a cost-effective renewable form through the sunlight reflection from an array of mirrors focused on a concentrated spot into a receiver/reactor, where the active material heats up and the reduction reaction occurs. The second step involves the reoxidation reaction, which is mildly exothermic and is favorable at lower temperatures. Temperature, partial pressure of oxygen, and concentration of gases play a key role in these reactions. The reduction reaction depends sensitively on temperature (T_R) and partial pressure of oxygen (p_{O_2}), with the degree of reduction or off-stoichiometry (δ) being a strong function of both variables, T and p_{O_2}. To avoid the reverse reaction, it is necessary to remove the oxygen released from metal oxide from the system prior to cooling in preparation for the reoxidation reaction. The reoxidation reaction highly depends on both temperature (T_{OX}) and the amount of excess reactant steam relative to available oxygen ion vacancies. The higher the reoxidation temperature, the larger amount of excess steam, whereas a lower reoxidation temperature requires shedding a large amount of sensible heat after the reduction step and then injecting a similar amount to raise the temperature of the material in preparation for another reduction step.

Unlike solar thermochemical water-splitting, in which two full redox reactions take place, photoelectrochemical water-splitting uses two half-reactions, e.g., hydrogen evolution reaction and oxygen evolution reaction.

While the overall water-splitting reaction is identical for both technologies, the STCH process involves two full reactions, where the two electrons left behind when removing an oxygen atom from the anion lattice nominally moves to the cation lattice within the solid-state MO_x material during the reduction reaction. As a result, the reduction reaction and reoxidation reactions in STCH are separated in time (temporally) and/or in space (spatially). Unlike STCH, in which two full redox reactions take place, PEC water-splitting uses two half-reactions, e.g., HER and OER. As a result, the two half-reactions must be performed simultaneously without any temporal separation. While the vast majority of the reported PEC water-splitting system performed HER and OER at the same rate,[13−18,46] additional redox couples or charge carriers can be introduced to the PEC device to replace either HER or OER for the spatial and temporal decoupling of hydrogen and oxygen generation.[47,48] It is also important to note that the reduction reaction or the oxidation reaction in PEC commonly refers to water reduction (eq 1) or water oxidation (eq 5), respectively. In contrast, for STCH the reduction reaction and the reoxidation reaction refers to the reduction and reoxidation of the redox materials and not of water. As a result, oxidation produces O_2 and H_2 in a PEC device and STCH reactor, respectively; while reduction produces the reverse, i.e., H_2 and O_2 in a PEC device and STCH reactor, respectively.

DEVICE/REACTOR ARCHITECTURE COMPARISON BETWEEN PHOTOELECTROCHEMICAL AND SOLAR THERMOCHEMICAL WATER-SPLITTING

The device architecture and reactor design in both PEC and STCH water-splitting are critical to the overall performance of the system. Two general types of PEC water-splitting device architectures, have been modeled and experimentally demonstrated at the laboratory scale.[4,49,50] A Type 1 PEC device indicates a system where the catalyst on a light absorber is configured in the form of particles suspended in the electrolyte, as shown in Figure 2a. Both a single chamber device, where hydrogen and oxygen coevolve, and a dual-chamber device, for which a redox shuttle is required in the Z scheme reaction, have been proposed and studied for particle-based systems. Based upon years of research on particle-based photocatalyst research, a flat panel-like, "catalyst sheet" device using Al doped $SrTiO_3$ was demonstrated in recent years at large solar collection area of ~1 m^2 that coevolved H_2 and O_2 at the catalyst surface.[51] While the Type 1 PEC device architecture has shown great promise in many technoeconomic analyses (TEA), the solar-to-hydrogen (STH) conversion efficiency is currently limited to <2%.[5,52,53] A Type 2 PEC device indicates a system for which catalyst coated planar semiconductor materials and membrane separators are configured to maximize the light absorption and to minimize the transport losses in the device with achievable STH efficiencies of about 20%.[13−18] Both PEC architectures can operate under ambient sunlight or relatively low concentration, e.g., a concentration factor C < 10. However, a recent development with a significantly higher concentration factor ($C \approx 474$) has also been demonstrated in a PEC system.[54]

For STCH, there are two conceptual reactor system designs: both reactions are placed in the same reactor or each one is placed in different reactors. In the first configuration (Figure 2c), the metal oxide remains in the same chamber and the reactions take place sequentially, hence temporal separation of O_2 and H_2. To have quasi-continuous hydrogen production and no to minimal waste of available solar radiation, two (or more) reactors are placed in parallel alternating between oxygen and hydrogen production.[29,55,56] For the second configuration (Figure 2d), the metal oxide moves from one reactor to the other and back again to the first. While the reduction reaction takes place in the on-sun reaction chamber, the reoxidation reaction takes place in an off-sun reaction

https://doi.org/10.1021/acsenergylett.1c00758
ACS Energy Lett. 2021, 6, 3096−3113

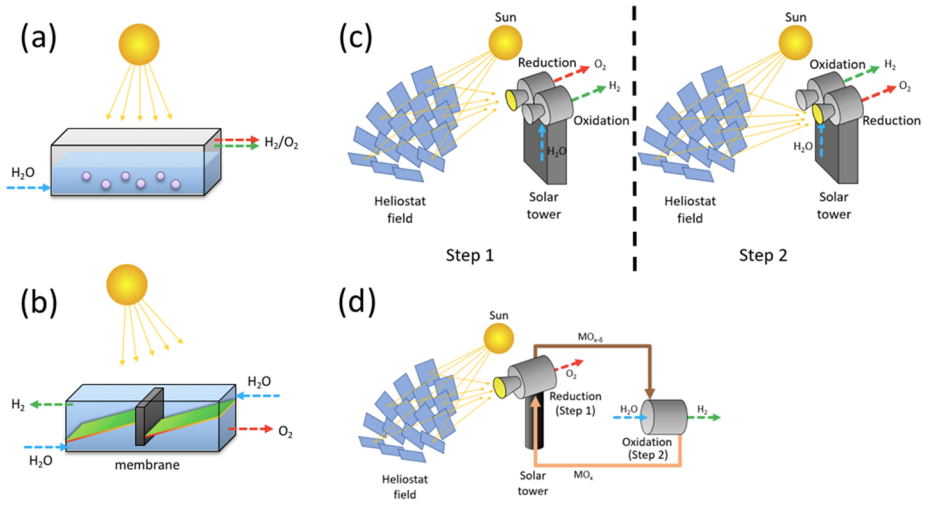

Figure 2. Schematic illustrations of device architectures for (a) particle-based PEC device, (b) planar catalyst-coated semiconductor PEC device, (c) two fixed-bed alternating reactors STCH system, and (d) moving particle STCH continuous production system.

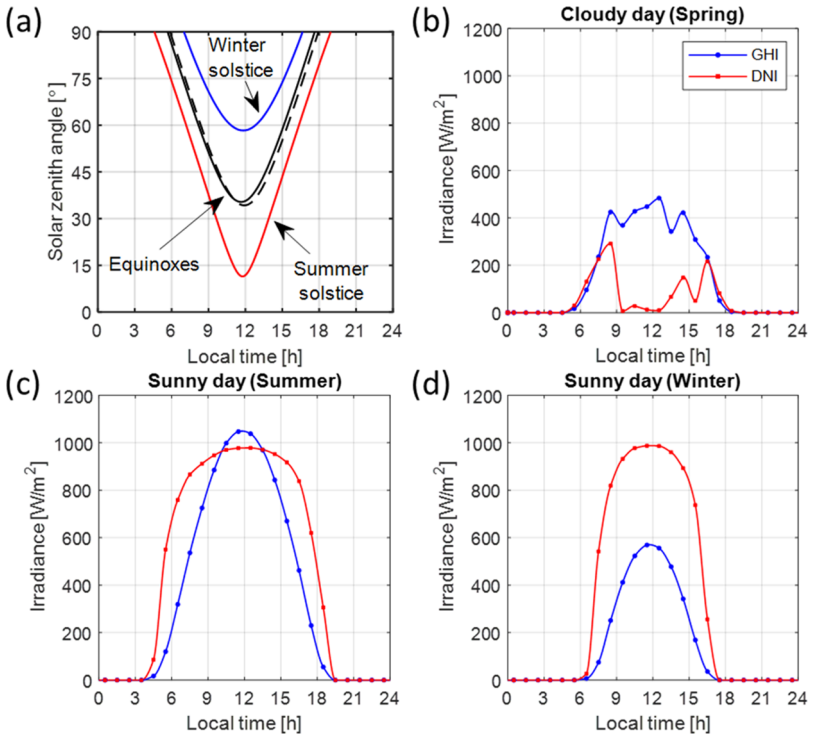

Figure 3. Daily variability of GHI and DNI in Daggett (CA). (a) Solar zenith angle daily variation for summer and winter solstices, and equinoxes. (b) Representative spring cloudy day (March 31, GHI = 3.87 and DNI = 1.31 kWh m^{-2} d^{-1}). (c) Representative summer sunny day (June 22, GHI = 8.91 and DNI = 11.65 kWh m^{-2} d^{-1}). (d) Representative winter sunny day (December 22, GHI = 3.87 and DNI = 1.31 kWh m^{-2} d^{-1}).

chamber. Thus, the production of H_2 is continuous and the separation of O_2 and H_2 is spatial. In addition, this configuration facilitates heat recovery, which is essential to obtain high efficiency. Technologically, the two main solutions proposed for this system concept are the moving bed of particles (or other form factor)[57,58] and the counter-rotating rings.[59,60] The moving particle concept has a higher operating flexibility since the particles can be stored and used on demand,[61] being possible to increase the capacity factor of the plant, however, that eliminates some opportunities for solid−solid heat recovery. The counter-rotating ring(s) reactor, on the other hand, simplifies the system by combining both reactors and the heat exchanger into a single device, but strongly couples the two reaction rates, limiting opportunities to independently vary the residence times for each reaction.

In PEC devices, the sunlight collection area is often comparable to the photoelectrochemically active area for the solar-driven water-splitting reaction, with the exception of solar concentrator coupled PEC devices, where the sunlight collection area is larger than the photoelectrodes by the concentration factor in the PEC device. As a result, the light absorber as well as the electrocatalysts for the water-splitting reaction often occupy a large geometric area in the system. For electrocatalysts, both uniformly coated, ultrathin catalyst layers

https://doi.org/10.1021/acsenergylett.1c00758
ACS Energy Lett. 2021, 6, 3096−3113

as well as dotted catalyst islands have been explored as viable approaches for efficient PEC devices for minimization of the parasitic light absorption. While the uniformly coated catalyst layer would occupy the same geometric area of the light capture area, the dotted catalyst islands could reduce the geometric area coverage by several orders of magnitude.[62,63] As a result, these designs with low filling fractions of electrocatalysts can significantly reduce the usage of precious metals. However, high-cost materials, such as RuO_x and IrO_x, even though they are stable and highly active for the oxygen evolution reaction in acid, are typically not encouraged for use in such systems due to the cost and scalability.[64] In contrast, STCH reactors require high concentration factors (at least 2500) to limit re-radiation losses ($\sim T^4$) that added to the collection losses, which are inclusive of optical losses, makes the collection area >5000 times larger than the receiver aperture area. The collected sunlight after the receiver focal point defocuses (generally) before falling on and being absorbed by the active materials in the reactor, which effectively has an absorbing flux at $C > 200-500$. In addition, the design context for a STCH reactor is typically for a centralized H_2 production plant; due to the balance of system cost, a minimal plant size is likely 1MW. In contrast, PEC owing to the panel-like modular design analogous to a PV panel, can be distributed with flexibility of plant size depending on the end use of the H_2.[49] While both will benefit from economies of scale, the expectation is that the minimum scale will differ between the two.

SUNLIGHT UTILIZATIONS OF PHOTOELECTROCHEMICAL AND SOLAR THERMOCHEMICAL SYSTEMS

While both PEC and STCH use sunlight to drive the water-splitting reaction, the sunlight utilization in each case is distinctively different. Direct normal irradiance (DNI), which is the power received on a unit area at the Earth's surface from the sun without having been scattered by the atmosphere, is the input sunlight power used for STCH, while global horizonal irradiance (GHI) represents the total amount of direct and diffuse radiation received from above by a horizonal surface is often used as the input sunlight power for PEC:

$$\mathrm{GHI} = \mathrm{DHI} + \mathrm{DNI}\cos(z) \tag{10}$$

where z is the solar zenith angle and DHI is the diffuse horizontal irradiance (power received on a unit area received from above by a horizonal surface DHI that does not arrive on a direct path from the sun). In sunny days, the DNI term represents up to 70−90% of the total irradiance; however, it is negligible on cloudy days.[65] The seasonal and daily variation resulting in larger z explains the higher annually average of DNI than GHI. As an example, Figure 3 illustrates this variation at Daggett (CA) based on hourly TMY2 (second edition of the typical meteorological year) data. The maximum annual variation in zenith angle occurs between the summer and winter solstices in nontropical areas as Figure 3a shows. At noon, the cosine factor attenuates the DNI in the GHI by 2% at the summer solstice and 47% at the winter solstice. This cosine factor explains the difference between DNI and GHI peaks in Figure 3c,d. Figure 3b shows the relevance of diffuse light during a cloudy day sometimes dominating GHI. The annual GHI and DNI in this representative sunny location are 2138 and 2791 kWh m^{-2}, respectively.

The preferred deployment sites for STCH or PEC is similar to concentrating solar power (CSP) or a traditional fixed PV panel, respectively. Only high insolation regions are preferred locations for STCH deployment with a recommended minimum annual DNI ≈ 2365 kWh m^{-2} yr^{-1} (6.5 kWh m^{-2} d^{-1}) and latitudes between 23 and 40° (north or south).[66] PEC offers more flexibility with locations owing to the contribution of diffuse light; however, locations closer to equator are beneficial with the lower zenith angle when tilt-tracker is not incorporated. The land-use requirements between PEC and STCH are comparable in the generation weighted average land use, and would likely follow a similar relationship as between PV and CSP.[67]

The AM 1.5G spectrum with an integrated power of 1000 W/m^2 is typically the standard input power spectrum for PEC cells. Both direct normal irradiance and diffuse (sky and ground reflected) contribute to the spectrum, collectable, in principle, from unconcentrated PEC device architectures. However, PEC devices coupled with solar concentrators with low concentrations would only be able to use the DNI, like STCH. In addition, depending on the light absorber materials, typical PEC devices only use part of the spectrum namely those photons with energies above the bandgap of the semiconductor materials, e.g., with enough energy $E_{ph} \geq E_g$. While the material strongly absorbs photons with energy much greater than the band gap, the resulting photogenerated electrons and holes typically thermalize back down to band edges before being transported to catalytic sites to drive fuel forming reactions, which translates to an energy loss. Figure 4a shows a prototypical solar spectrum utilization for a tandem PEC (for instance InGaP/GaAs cell with a bandgap combination of 1.78 and 1.26 eV). The total power of AM 1.5 spectrum is 1000 W m^{-2} while the maximum power constrained by the bandgap is 729 W m^{-2} before considering thermalization losses (describe in the later paragraph), corresponding to 27.1% loss.

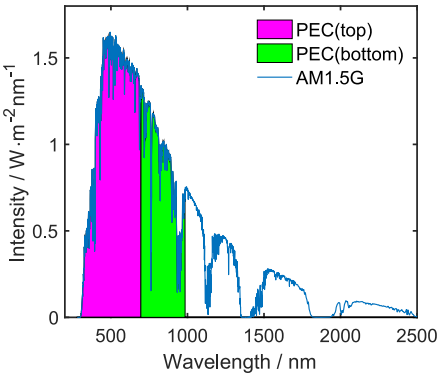

Figure 4. AM 1.5G spectrum with the band gaps of the dual-junction light absorber defining the wavelength region of interest for the PEC system (pink color for top cell and green color for bottom cell).

In contrast, STCH uses the whole spectrum; however, the concentrating technology introduces collection losses before the radiation reaches the reactor. Assuming power tower technology, these losses depend on many varied factors including the position of sun, the location of the individual heliostat relative to the receiver, and the sizes of the heliostat and the receiver aperture. Among the most common losses considered are reflection losses, cosine factor, shading and

https://doi.org/10.1021/acsenergylett.1c00758
ACS Energy Lett. 2021, 6, 3096−3113

blocking, atmospheric attenuation, and receiver spillage. A total of 40−60% of the collected energy reaches the external surface of the receiver aperture,[56,61] and of that, 5−35% is lost from re-radiation and convection with the environment due to the high temperature in the solar receiver (reduction reactor).[61,68] Note that re-radiation and convection losses are highly dependent on the temperature and the concentration ratio, as shown in Figure S1. Due to these energy losses before any radiation can be used in the reduction reaction, a minimum insolation threshold in the vicinity of 300 W m^{-2} is typically necessary for system operation.[68] At Daggett, for example, 95% of the available solar energy is above this threshold value.

SOLAR-TO-HYDROGEN CONVERSION EFFICIENCY DEFINITION OF PHOTOELECTROCHEMICAL AND SOLAR THERMOCHEMICAL SYSTEMS

Among various performance metrics, the solar-to-hydrogen (STH) conversion efficiency is one of the most important parameters in determining the levelized hydrogen production cost.[4,69] In particular, high STH conversion efficiency alleviates the land requirements for a given hydrogen production capacity (e.g., kg/day) and lowers the balance of system cost. In both PEC and STCH systems, the STH conversion efficiency is not only dependent on the active materials, but also on the cell or reactor designs. For STCH, the STH also depends strongly on the mirror collection configuration, which determines the collection efficiency. The most efficient is not necessarily the most cost-effective, which is an important consideration.

The definition of the STH conversion efficiency is the ratio of the work that the chemical product (hydrogen) can perform to the overall energy input (solar) to produce the product. Here, we conceptually include a fuel cell at the exit of both systems as it allows the combined system to be modeled as a work producing power cycle. Note that the definition of the STH conversion efficiency includes a time duration, e.g., an hour, a day, or a year. When the analysis of the system is just for an infinitesimal unit of time, then the instantaneous STH conversion efficiency can be defined as the ratio of the power that can be extracted from the chemical product (hydrogen) to the overall power input to produce it (solar) at that instant.

Table 1 lists the relevant energies associated with water and hydrogen, including the standard Gibbs free energy of formation for liquid water (ΔG_l^0) and water vapor (ΔG_g^0), the standard formation enthalpy for liquid water (ΔH_l^0, or the higher heating value of hydrogen, HHV) and water vapor (ΔH_g^0, or the lower heating value of hydrogen, LHV), vaporization energy (W_{vap}), and isothermal and adiabatic compression energy (W_{comp_iso} and W_{comp_adi}). Confusion with values and definitions can lead to mistakes in calculation of the STH efficiency or incorrect comparisons. We also converted the energies into different units to make the comparison as clear as possible.

Table 1. Lists of Standard Gibbs Free Energy of Formation (ΔG^0), Standard Enthalpy of Formation (ΔH^0), Vaporization Energy (W_{vap}), and Isothermal and Adiabatic Compression Energy (W_{comp})[70,71]

	T (K)/P (bar)[a]	phase of water	kJ/mol H_2	kWh/kg H_2	eV
ΔG_l^0	298/1	liquid	237.1	32.7	1.23
ΔH_l^0 (HHV)	298/1	liquid	285.8	39.4	1.48
ΔG_g^0	298/1	gas	228.6	31.4	1.18
ΔH_g^0 (LHV)	298/1	gas	241.8	33.3	1.25
W_{vap}	298/1	liquid to gas	44.0	6.1	0.23
W_{comp_iso}	298/1 to 298/350	gas	14.5	2.0	0.08
W_{comp_adi}	298/1 to 1637/350	gas	38.3	5.3	0.20

[a]The pressure of 350 bar is commonly applied in fuel cells.

We define the STH conversion efficiency for both systems, PEC and STCH, as

$$\eta_{STH\ (PEC\ and\ STCH)} = \frac{n_{H_2}\ (mol)\ \Delta G_l^0\ (kJ\ mol^{-1})}{Q_{solar}\ (kJ)} = \frac{m_{H_2}\ (kg)\ \Delta G_l^0\ (kWh\ kg^{-1})}{Q_{solar}\ (kWh)} \quad (11)$$

where n_{H_2} and m_{H_2} are the amount of hydrogen produced over a unit of time in mol and kg, respectively, ΔG_l^0 is the Gibbs free energy of water formation in the liquid phase, and Q_{solar} is the incident solar energy over the same unit of time. Note that the maximum net work that can be extracted from the chemical product is defined by ΔG_l^0. When the purpose of the H_2 is the heat of combustion as opposed to net work, then that can be extracted from it, HHV (if the water condenses in the process) or LHV (if the water does not condense in the process) should be used in the STH leading to higher efficiencies than the maximum work metric. Equation 12 shows the instantaneous STH conversion efficiency:

$$\eta_{STH,inst} = \frac{\dot{n}_{H_2}\ (mol\ s^{-1})\ \Delta G_l^0\ (kJ\ mol^{-1})}{\dot{Q}_{solar}\ (kJ\ s^{-1})} = \frac{\dot{m}_{H_2}\ (kg\ s^{-1})\ \Delta G_l^0\ (kWh\ kg^{-1})}{3600\dot{Q}_{solar}\ (kW)} \quad (12)$$

where $\dot{n}_{H_2}$ and $\dot{m}_{H_2}$ are the molar and mass flows, respectively, of hydrogen produced at this specific moment and $\dot{Q}_{solar}$ is the incident solar flux.

In PEC systems, Q_{solar} is defined as the total solar energy that reaches the photoactive part of the PEC device. We note that the sunlight collection area in PEC devices is often comparable to the photoelectrochemically active area. The instantaneous STH conversion efficiency device is often evaluated as follows:

$$\eta_{STH,inst(PEC)} = \frac{\Delta U_{rxn}\ (V)\ J_{op}\ (mA\ cm^{-2})\ f_{FE}\ (\%)}{P_{light}\ (mW\ cm^{-2})} = \frac{1.23\ V \times J_{op}\ (mA\ cm^{-2})\ f_{FE}\ (\%)}{100\ mW\ cm^{-2}} \quad (13)$$

where J_{op} is the PEC operating current density at 0 V vs counter electrode potential, ΔU_{rxn} = 1.23 V is the thermodynamic potential for water-splitting, f_{FE} is the reaction Faradaic efficiency, and P_{light} is the incident light irradiance. Equation 11 is often used to evaluate the daily or annually averaged STH conversion efficiency for PEC devices.

From the energy efficiency point of view, the vast majority of the energy loss in the PEC system takes place within the PEC devices (particle-based devices or planar catalyst coated semiconductor based devices). The energy requirements in

https://doi.org/10.1021/acsenergylett.1c00758
ACS Energy Lett. 2021, 6, 3096−3113

the balance of system (BOS) for the PEC system are low. For example, optical components or heat management would not be needed for unconcentrated PEC devices at the system level. The energy requirements for pumping or circulation of electrolytes within PEC devices are minimal at the system level. In addition, the product separation, which could require significant energy inputs in STCH, is often not a concern and would not need additional energy inputs in PEC systems due to the incorporation of membrane separators. As a result, scaling up of PEC devices can often be achieved by multiplexing and connecting unit cells, and this approach was demonstrated in literature showing comparable performance as a single cell.[72,73] Note that while the energy requirements for PEC's BOS is low, the cost related to BOS is not necessarily low.

In STCH systems, the energy used to produce the hydrogen necessarily includes energy collected by the concentrating mirrors (typically a heliostat field but can also be a parabolic dish concentrator) to project redirect the sunlight into a receiver, but can include an additional contribution of energy to cover a series of the parasitic loads needed to drive the process. Among these loads, the most significant are the receiver oxygen removal, the H_2-H_2O separation work, and the steam generation. Depending on the chosen operating conditions, the energy recovery system can or cannot cover the total demand of energy. Thus, when internal heat is insufficient, then it is necessary to include these added energy contributions in the STH definition. Note that the primary energy resource to provide these parasitic loads may or may not be from a solar origin, but for practical reasons it is considered solar as the solar equivalent in the STH definition. Hence, the STCH community often expresses the STH conversion efficiency as follows:

$$\eta_{\mathrm{STH(STCH)}} = \frac{n_{\mathrm{H_2}}\ (\mathrm{mol})\ \Delta G_{\mathrm{l}}^{0}\ (\mathrm{kJ\ mol^{-1}})}{Q_{\mathrm{solar}}\ (\mathrm{kJ}) + Q_{\mathrm{aux}}\ (\mathrm{kJ})} = \frac{m_{\mathrm{H_2}}\ (\mathrm{kg})\ \Delta G_{\mathrm{l}}^{0}\ (\mathrm{kWh\ kg^{-1}})}{Q_{\mathrm{solar}}\ (\mathrm{kWh}) + Q_{\mathrm{aux}}\ (\mathrm{kWh})} \quad (14)$$

where Q_{solar} is the incident solar energy calculated as the integral of incident solar flux over the time duration analyzed and Q_{aux} is the added energy input to cover the parasitic loads of the process over the same time duration. There is no consensus in the STCH community regarding Q_{solar}, some researchers include the process of solar collection and others not. To make a fair comparison with PEC systems, we define Q_{solar} as the total solar energy that reaches the collection area; therefore, the collection losses and receiver re-radiation and thermal losses are included in this definition.

It is important to note that, while different definitions of the solar-to-hydrogen conversion efficiency have their own merits in guiding the development of the technology in the field, simple comparisons between these efficiency numbers with different definitions could be misleading.

It is important to note, that while different definitions of the STH conversion efficiency (for example, the different expression of STH conversion efficiency in eqs 11 and 14) have their own merits in guiding the development of the technology in the field, simple comparisons between these efficiency numbers with different definitions could be misleading. In addition, while the Gibbs free energy, which represents the maximum extractable net work from the chemical products, should be used in the numerator in the efficiency definition, the use of $\Delta G_{\mathrm{l}}^{0}$ or $\Delta G_{\mathrm{g}}^{0}$ depends on the phase of the water at the system boundary. To compare between PEC and STCH, we consider various power losses as the input power from sunlight goes through the PEC and STCH system. For PEC, we examined the loss mechanism in a high-efficiency PEC device[14] as illustrated in Figure 5a,b. See details of the quantification in Figures S2 and S3.

Figure 5a starts from a standard AM1.5G illumination with solar power of 1000 W m^{-2} as design point (DP). Since the photoabsorber can only absorb photons with energies greater than the specific bandgap, for the InGaP/GaAs tandem cell, 729 W m^{-2} of power is usable, which corresponds to 27.1% loss from the spectrum below bandgap.[14] The second power loss originates from the less than perfect reflectivity due to the materials in the optical pathway, such as catalyst or protective layers. In this case, an additional 7.4% is lost leading to 655 W m^{-2} in the remaining power.[14] The third power loss comes from the thermalization and recombination loss within the photoabsorber at the operating voltage and current density. For the PEC assembly using InGaP/GaAs tandem photoabsorber and RuO_2/Rh NP catalysts for OER and HER, the operating current density, voltage, and resulting power are 15.7 mA cm^{-2}, 1.93 V, and 303 W m^{-2}, respectively.[14] The calculated thermalization and recombination loss is 35.2% of the total incident solar power. The energy output of PEC water-splitting device is then limited by Gibbs free energy of water formation. Hence, the last power loss can be contributed to catalysis loss from the overpotentials for water-splitting catalysis as well as polarization losses such as resistive loss due to ionic transport in the PEC device. With the addition of 11% electrocatalysis loss of the total incident solar power, the resulting hydrogen generation power from in the reported PEC assembly is 193 W m^{-2}, leading to a 19.3% STH conversion efficiency.[14]

The thermalization and recombination loss is the major loss that is constrained by the detail balance limit (or Shockley–Queisser limit). However, bandgap optimization can improve the device efficiency. Note that further reduction of the electrocatalytic loss based on RuO_2 (for OER)/Rh NP (for HER) catalysts will result in minimal improvement in the STH conversion efficiency of the PEC assembly using InGaP/GaAs tandem photoabsorber based on the load curve analysis (see Figure S2). Replacing the catalysts with nonprecious metal catalysts will further increase the electrocatalytic losses and also results in significant decrease in the STH conversion efficiency of the system because the operating points move sharply beyond the maximum power point of the PV curve. Different tandem structures or triple junction cells with optimal combination of bandgap values would be desirable to accommodate reduction of the electrocatalytic activity of the catalysts.[74] Figure 5b shows our results from an annual average based on GHI irradiance in Daggett (CA). Starting with average solar power of 244 W m^{-2}, the 27.1% below bandgap photon loss leads to remaining power of 178 W m^{-2}. After

https://doi.org/10.1021/acsenergylett.1c00758
ACS Energy Lett. 2021, 6, 3096–3113

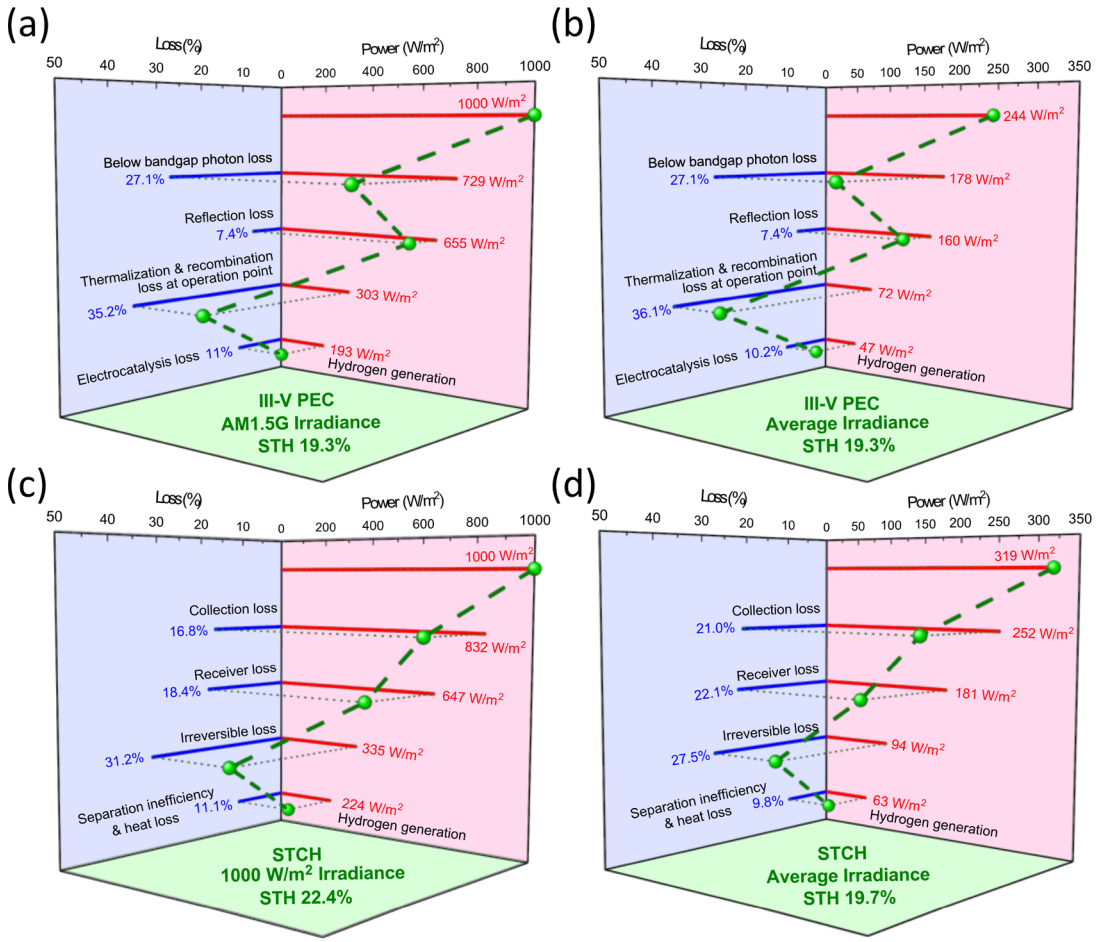

Figure 5. Comparative examples of STH conversion efficiency and power loss analysis between (a) PEC with AM1.5G irradiance, (b) PEC with annual GHI irradiance in Daggett (CA), (c) STCH with 1000 W/m^2 irradiance, and (d) STCH with annual DNI irradiance in Daggett (CA).

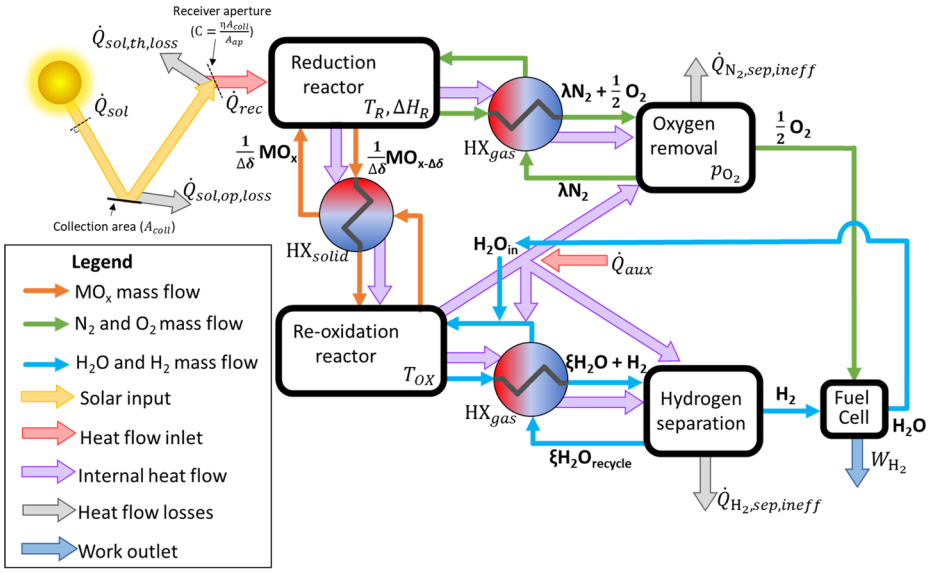

Figure 6. Schematic system diagram of the moving particle STCH system including mass flows (thin arrows) and heat flows (thick arrows).

considering 7.4% from reflection loss, we obtain a power of 160 W m^{-2}. With the additional thermalization and recombination loss of 36.1%, 72 W m^{-2} remains to contribute to hydrogen generation. Lastly, we account for the 10.2% electrocatalysis loss. As the production rate of hydrogen scales linearly with the solar illumination in the optimized coupling between the light absorber and catalysts, the annual averaged STH conversion efficiency in the system considered here

https://doi.org/10.1021/acsenergylett.1c00758
ACS Energy Lett. 2021, 6, 3096−3113

yielded the same STH efficiency as the instantaneous STH conversion efficiency at the DP of 19.3%, with the hydrogen generating power going down to 47 W m^{-2}, corresponding to an annual 411 kWh m^{-2} yr^{-1}. In other words, the losses are not dependent on the absolute illumination, in contrast to STCH, where some losses scale with illumination and others are fixed independent of illumination. Hence, the annual average efficiency in STCH differs from peak efficiency noticeably (see below).

As pointed out earlier, the high STH conversion efficiency does not necessarily lead to the low cost of H_2. Si-based cells in PEC are also considered promising despite the limitation on the attainable STH conversion efficiency. Figure S4a evaluated the loss of a 4.7% Si-based PEC device using earth-abundant electrocatalyst materials.[15,75] The below bandgap loss, reflection loss, thermalization and recombination loos, electrocatalysis loss accounted for 16.4%, 35%, 42.5%, and 1.4%, respectively (Figure S4a).

Due to the low technology readiness level (TRL 2−4[76]), the STH conversion efficiency of STCH plants is usually estimated through process simulation.[40,76] Many studies have proposed their own models obtaining different results as a consequence of applying different assumptions. The results presented here are representative of a continuous production (moving-particles) STCH system with CeO_2 as the redox-active material[77] (see Figure 6). In the analyzed system, the active material (orange thin arrows) moves in a loop between reduction, solid−solid heat exchanger, and reoxidation reactor; the N_2 (green thin arrows) moves in a loop between the reduction reactor, gas−gas heat exchanger, and O_2 removal system; and H_2O (blue thin arrows) moves in a loop between the reoxidation reactor, gas−gas heat exchanger, H_2 separation system and fuel cell. The solar technology used for the purposes here is a solar dish and a concentration ratio of 5000 suns.[78] The production system consists of two countercurrent reactors one each for reduction (oxygen production) and reoxidation (hydrogen production). Underlying assumptions are that heat recovery can have an effectiveness of 85% between solid particles (solid−solid) and 95% between gases (gas−gas),[68] and the separation efficiency is ∼10% with respect to the minimum required for an ideal separation process.[79,80] For the purposes here, the oxygen removal technology is a nitrogen sweep gas with an initial partial pressure of oxygen of 10 Pa (∼100 ppm at a standard atmosphere), a N_2/H_2 molar flow ratio of 5 and a conversion yield (H_2 product/H_2O reactant) of 10%. Both nitrogen and excess steam recycle after the reaction and after separating the produced oxygen and hydrogen, respectively. The excess heat (from the exotherm of the reaction) in the reoxidation reactor can serve as input heat to downstream processes that occur at a temperature lower than the reoxidation temperature (such as producing steam from liquid water, in an oxygen removal device, and/or for the hydrogen separation); if insufficient, an auxiliary heat contribution completes the energy balance. For the purposes of illustration, the operating temperatures selected are 1700 and 950 °C for reduction and reoxidation, respectively.

Figure 5c,d shows the energy loss mechanisms in the selected STCH system. Figure 5c starts from a solar irradiance at a DP of 1000 W m^{-2}, a typical DNI value reached at noon on a clear day. As soon as the sunlight reaches the surface of the solar collector, there are a series of collection losses, which reduce the solar irradiance entering the receiver. First, the reflectivity and the cleanness of the mirrors used to concentrate the sunlight is not perfect and the mirror only reflects 87.5% of the incident sunlight (here, we are assuming 95% for reflectivity, 95% for soiling, and 97% for the surface reflective ratio).[81] Once the concentrated light reaches the aperture of the receiver, only part of the radiation falls within the aperture (here we are assuming 95%).[78] The aperture intercept is the trade-off between maximizing the radiation entering the receiver and minimizing the re-radiation losses from the receiver.[68] At the DP, the sum of all these collection losses is ∼16.8% of the total irradiance. Note that if the solar collection technology is a heliostat field, the collection losses also include a cosine factor, shading and blocking, and attenuation from the atmosphere between the mirrors and the receiver.[81]

Once the concentrated sunlight reaches the aperture of the receiver, another series of losses related with the receiver affects the remaining solar irradiance. The receiver/reactor requires a controlled atmosphere and thus uses a transparent window over the aperture to isolate the reactor from ambient conditions. The transparency of this window is not perfect, which results in a loss of ∼5% of the impinging radiation.[68] The receiver losses also include thermal losses from the receiver to the environment dominated by re-radiation, which scales as the fourth power of the temperature, assuming no active window cooling required, which considerably reduces convective losses.[59,82] The reduction reaction occurs at a high temperature, and although we can reasonably assume that the receiver is perfectly insulated the aperture of the receiver is necessarily exposed to the environment.[68] At the DP, the sum of the receiver losses depends on the concentration ratio and the re-radiation temperature; with the assumptions here (1700 °C and 5000 suns, which is equivalent to 5 MW m^{-2}) is ∼18.4% of the total irradiance, hence the irradiance that reaches the redox-active material is ∼647 W m^{-2}. The material absorbs the radiation (ideally the material is close to a perfect absorber), which causes the material to heat and as it heats the redox-active off-stoichiometric metal oxide reduces and releases oxygen (electrons from the oxygen anion stay behind and find a receptive cation to reduce). The absorbed energy is necessarily more than enough to split water. Hence, the second reaction step is exothermic.

The balance of system has a number of energy consuming processes that are important in estimating an overall system efficiency. Among the inevitable energy consumption of the system are the ΔH of reduction for the material and the free energy of mixing of the gases (N_2/O_2 and Steam/H_2). However, since the unit operations of O_2 and H_2 separations occur at lower temperatures than the reoxidation temperature, the rejected heat (and exergy) from the reoxidation exotherm. Therefore, ΔH of reduction is the minimum energy needed to drive the thermochemical process. Considering only this energy expenditure, the thermochemical process efficiency is ∼51.7% accounting for 31.2% of the losses of the total irradiance. Note that this value is dependent on the active material, here ceria, and the operating conditions of the system. Including realistic separation inefficiencies and heat transfer exergy destruction, the thermochemical process efficiency drops to 34.6%. The heat recovery here reuses the unrecovered particle sensible heat in the solid−solid heat exchanger and the exothermic heat of reaction released in the reoxidation to heat the reactants and to supply the energy demand of separations of the product gases O_2 and H_2 from

https://doi.org/10.1021/acsenergylett.1c00758
ACS Energy Lett. 2021, 6, 3096−3113

nitrogen and excess steam, respectively. When this energy balance is not sufficient, then an input of energy must be added ($\dot{Q}_{aux}$) which in this example was not necessary.

Figure 7 shows the internal energy distribution for a STCH system based on ceria at the DP and inevitable inefficiencies. In

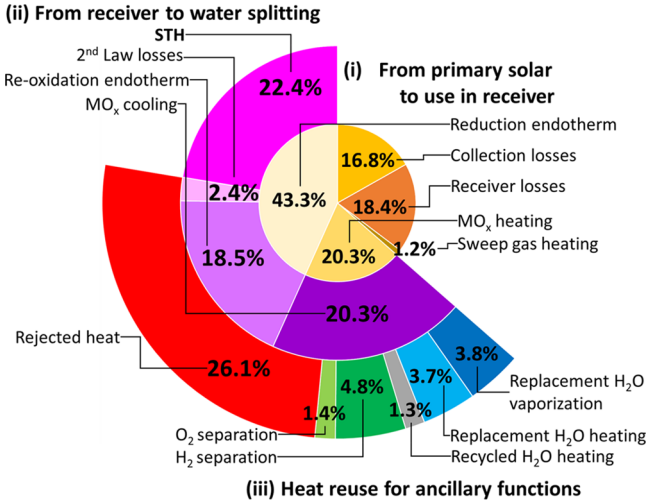

Figure 7. Energy distribution in a STCH system at the design point: (i) from primary solar on the focusing mirrors for use in the receiver, (ii) from the receiver to water-splitting reoxidation reactor and (iii) heat reuse for ancillary functions.

this example, the heat absorbed in the receiver is divided into three terms: one to provide the reduction endotherm to make the reaction possible (43.3% of total) and two to compensate for imperfect heat exchanger effectiveness heating both the sweep gas and metal oxide to the reduction temperature (1.2% and 20.3% of the total energy input for the gas and solid, respectively). The metal oxides carry the energy captured in the reduction reactor to the reoxidation reactor. Here, we can account for four terms: one part is used to produce hydrogen (22.4%), a second part is the heat released by the exothermic reaction (18.5%), a third part is sensible heat released to compensate for imperfect heat exchanger effectiveness on cooling (20.3%), and the final part is second law necessary loss in heat to H_2 conversion (2.4%). The heat not converted into H_2 in the reoxidation step is available to drive all the remaining auxiliary processes at lower temperature than the reoxidation temperature.[68] In our example here, the vaporization of the water consumed in the reoxidation is 3.8% of the total energy input. The heating of this steam and the recycled steam from the steam–H_2 separation process to the reoxidation temperature is 3.7% and 1.3% of the energy expenditure, respectively. The separation of the H_2 and O_2 consumes 4.8% and 1.4% of the total energy input, respectively. The remaining energy is rejected heat, which accounts for 26.1% of the total energy consumption and is available for use in other processes such as electricity production.[7,83] At the end of the STCH process, the resulting H_2 generation power in the selected STCH system is 224 W m^{-2}, leading to a 22.4% STH peak conversion efficiency. Other redox-active materials with lower ΔH of reduction than ceria could lead to higher STH conversion efficiencies.

When the DNI is lower than the DP (i.e., 1000 W m^{-2}), the efficiency decreases because some losses are constants and do not scale with the DNI. Figure 5d shows our results from an annual average based on DNI irradiance in Daggett, California. Starting with average solar power of 319 W m^{-2}, the annual average STH conversion efficiency for this ceria example is 19.7%. Due to energy losses in the process, the system requires a minimum insolation level to operate. Taking a conservative value of 300 W m^{-2}, ~95% of the available solar energy is above this minimum threshold. The annual collection losses account for 21.0% of the total energy input. Heat losses from the receiver increase when the concentrated irradiance is under the DP DNI; hence, the annual average receiver losses increase to 22.1% of the total losses. The thermochemical process efficiency remains constant because a well-designed operating control system would adjust the particle flow to the amount of radiation and because we are not considering losses from thermal inertia in the reactors and heat exchangers at this level of analysis. The annual thermochemical process losses account for ~37.3% of the total annual energy input.

If the solar technology used for the energy collection is a heliostat field with a solar tower instead of a parabolic dish, the efficiency will be lower for both the DP and the annual basis, due to several factors. Among these factors, most significant are the cosine effect factor for the heliostat field (i.e., the reduction of the effective reflection area because heliostats do not point directly at the sun), the atmospheric attenuation, the shading and blocking of the heliostats at some solar angles, and a higher receiver spillage (lower interception). The typical collection efficiency at the DP is 60%, and the concentration ratio for thermochemical applications is 3000 (sometimes including secondary concentrators, with additional collection losses; hence, there is a trade-off between collection efficiency and receiver efficiency when determining the optimal concentration factor for performance and cost). The major factor in designing an optimized heliostat field layout is the cosine "efficiency" of the heliostat. This efficiency depends on both the sun's position and the location of the individual heliostat relative to the receiver. A tracking mechanism positions the heliostat so that its surface normal bisects the angle between the sun's rays and a line from the heliostat to the tower. The effective reflection area of the heliostat, as a result, is reduced by the cosine of one-half of this angle. A less-optimistic scenario of the STCH based on heliostat field technology, a reduction temperature of 1500 °C, and a solid–solid effectiveness of 70% is included in Table S1. Figure S4b evaluates this less-optimistic scenario resulting in a 5.8% STH conversion efficiency at the DP. However, it is important to highlight that CeO_2 is too difficult to reduce and the extent of reduction at 1500 °C is low, penalizing the system performance. Other materials with better reduction capability could significantly increase this STH conversion efficiency, which is where much of the forefront research is ongoing.

Another figure of merit to use for the conversion efficiency for both technologies is the energy utilization number, $U = \frac{Q_{total}\ (kWh)}{m_{H_2}\ (kg)}$, which refers to the total energy required to produce

Another figure of merit to use for the conversion efficiency for both technologies is the energy utilization number, which refers to the total energy required to produce 1 kg of H_2 at standard temperature and pressure.

https://doi.org/10.1021/acsenergylett.1c00758
ACS Energy Lett. 2021, 6, 3096–3113

Table 2. Summary of Operating Conditions for PEC and STCH Systems

	photoelectrochemical (PEC)	solar thermochemical (STCH)
operating temperature	5 to 80 °C	reduction: 1350−1800 °C reoxidation: 600−1250 °C
illumination intensity	0 mW cm^{-2} to 1 W cm^{-2} up to 47.4 W cm^{-2}	focal point: $C \approx 2500-5000$ suns (2.5−5 MW m^{-2}) absorbing material: 20−50 W cm^{-2}
water condition and utilization	liquid water or water vapor at ambient T and P; recirculate water/electrolyte during operation	steam at or below the oxidation temperature and typically 1 bar, use water−steam transformation, preferred 90% steam or below after reaction; recirculate the excess steam after separating the H_2
hydrogen output	humidified H_2 at ambient temperature (before separation)	H_2−steam mixture (0.1 bar or higher) at the oxidation temperature (before separation)
impact of partial pressure of O_2	10^{-4} bar (corresponds to 240 mV)	10−100 Pa (10^{-4}−10^{-3} bar) in the reduction reaction to increase reduction extent
capacity factor	24.4% in Daggett, CA, generally ∼15−30%	28.1% in Daggett, CA, without storage, preferred range 25.7−100%
spatial and temporal constraints	constrained by the lowest rate of reduction and oxidation	two different reduction and reoxidation reactions that are spatially or temporally separated; different reduction and reoxidation rates possible
potential sites	potentially deployable over oceanwater, PV screening	DNI > 6.5 kWh m^{-2} day^{-1}; land use; CSP screening

1 kg of H_2 at standard temperature and pressure. For the InGaP/GaAs cell with 19.3% STH conversion efficiency, U = 183 kWh kg^{-1} H_2. With the annual GHI of 2138 kWh m^{-2} in Daggett, CA, an average H_2 production rate of 0.032 kg day^{-1} m^{-2} is feasible. It is important to note that the energy utilization number is also dependent on the final state of the H_2; for instance, Table 1 shows a calculated difference of 5.3 kWh kg^{-1} H_2 between H_2 at 1 and 350 bar in an adiabatic pressurization process. For a STCH system with 19.7% annual STH conversion efficiency, U = 166 kWh kg^{-1} H_2. With the annual DNI of 2791 kWh m^{-2} in Daggett, CA, an average H_2 production rate of 0.046 kg day^{-1} m^{-2} is feasible; note that this result is for collection area, not for total land area.

OPERATING CONDITIONS FOR PHOTOELECTROCHEMICAL AND SOLAR THERMOCHEMICAL SYSTEMS

Table 2 summarizes the differences in operating conditions between PEC and STCH systems. Most reported lab-scale PEC devices operate at room temperature under various illumination conditions without careful control over the operating temperature of the device. However, in the real-world PEC devices will likely need to operate above the freezing point of the electrolyte, or 80 °C under concentrated sunlight. The trade-offs of operating at elevated temperature have been investigated.[84−86] While the increased temperature improves the kinetics for the water-splitting reaction, it also has detrimental effects on the performance of the photoabsorber.[84−86] In contrast, STCH operates at two different temperatures, one temperature for each reaction: 1350 °C to as high as 1800 °C in the reduction reactor (oxygen production) and 600−1250 °C in the reoxidation reactor (H_2 production). The choice of these temperatures is a critical factor in the STH conversion efficiency. On the one hand, a high reduction temperature favors oxygen production from the redox-active material, while a low reoxidation temperature favors H_2 production and reduces the excess steam requirements. On the other hand, the temperature gap increases the heat requirements of the cycle, challenging the efficiency even with a fairly high (as used here) heat recovery effectiveness. The optimal values depend on the thermodynamics of the redox-active metal oxide used.

PEC devices can operate at a wide range of illumination intensities from close to zero illumination to as high as 474 W m^{-2}.[54] Proper thermal management is required under high illumination conditions. Operation under high illumination conditions significantly reduces the materials costs associated with photoabsorbers but also requires more active electrocatalyst materials to operate at high productivity rates. STCH systems require high illumination conditions (highly concentrated) to limit re-radiation from the high-temperature reduction reaction. However, that illumination is typically not the illumination onto the active materials. A minimum DNI threshold is typically necessary to ensure that the receiver does not hit a stagnation temperature lower than the desired reduction temperature. Note that the higher the concentration ratio, the lower the receiver re-radiation losses, but typically accompanied by a higher cost for the solar collection; therefore, it is a design parameter that should be optimized in a techno-economic analysis. In other words, the highest efficiency system is not necessarily the most cost-effective.

PEC devices use liquid water or water vapor as the input water feedstock.[87] For liquid water, various types of electrolytes including acid, base, or near-neutral pH electrolytes have been employed, and each has its own advantages and disadvantages.[14,88−90] Water vapor has also been used in the design of PEC water-splitting devices, where no bulk liquid water is required for the sustained cell operation.[87] The water does not go through phase changes in the PEC device and is often recirculated in the device to minimize any pH gradients at the electrode surface and electrodialysis losses in the cell.[91] The energy required to recirculate water or electrolyte is negligible in comparison with energy losses associated with kinetic overpotentials for catalysts or overall water-splitting reactions.[92] STCH systems use superheated steam typically at atmospheric pressure. The reoxidation reaction depends sensitively on both temperature and the amount of excess steam relative to available oxygen ion vacancies. The higher the reoxidation temperature, the larger the amount of excess steam needed to drive the reaction to near completion, whereas a lower reoxidation temperature requires a large amount of sensible heat to be shed after the reduction step and then injected to raise the temperature of the metal oxide for the reduction step. Steam recirculation (avoiding the phase change as discussed above for PEC) and high heat recovery effectiveness are critical to reduce the heat system requirements.

https://doi.org/10.1021/acsenergylett.1c00758
ACS Energy Lett. 2021, 6, 3096−3113

The H_2 produced from PEC devices is often humidified, and additional processes will be required to remove the water vapor from H_2; however, the output H_2 is relatively pure, with minimal gas impurities such as O_2. In STCH systems, the production of H_2 is at the reoxidation temperature (600−1250 °C) in a mixture of excess steam. The process for separation of H_2 from the steam−H_2 mix contributes to the total energy consumption. Optimizing the temperature and approach to the H_2/H_2O separation will be important; however, to date there has not been much research attention to this important part of the system. The lower the separation temperature, the lower the theoretical energy of separation. Nevertheless, the lower the separation temperature, the greater the demand on gas−gas heat recovery or recovery of the vaporization energy if the steam condenses. There is a reasonable consensus in the STCH community that avoiding the gas-to-liquid phase transition and doing the separation in the gas phase will require less overall energy demand. After separating the H_2, it will be necessary to pump it up to the required delivery pressure.

The partial pressure of O_2 in the anode chamber for the PEC device will change the equilibrium potential for OER, and as a result, the required total voltage for water-splitting will be reduced as the partial pressure of O_2 decreases in the anode chamber. For example, if the partial pressure of O_2 is 10^{-4} bar, the total voltage for the water-splitting reaction reduces by ∼240 mV based on the Nernstian relation. Oxygen removal is another critical aspect of STCH systems. A reduced O_2 partial pressure is a requirement in the reduction reactor to increase the reaction extent for the oxides (as it increases the entropy production for the oxygen to go from bound in the lattice to the gas phase). The current metal oxide materials suggest partial pressures of 10−100 Pa will be necessary (lower is desirable, but reducing the partial pressure has a number of associated challenges). Although lower partial pressures increase the extent of reduction (the amount of off-stoichiometry), it also introduces an engineering challenge, and considerations of the rapidly increasing volume flow will determine ultimate limitations. Vacuum pumping and inert gas sweeping are the main technologies to achieve these low oxygen partial pressures, and both have advantages and disadvantages discussed in the literature.[79,93] Alternatives that are also being explored recently include thermochemical pumping and sorption pumping/separation.[80,94]

The capacity factor, defined as the ratio between the actual energy output and output if operated at maximum capacity at all times, is quite similar for PEC and STCH, as they are both direct solar technologies and operate when the sun is shining. For PEC devices, the overall rate of H_2 production is constrained by the lower of the two rates, water oxidation or proton reduction. In other words, the OER at the anode and HER at the cathode must always be rate-matched. Note that it is possible to achieve a higher overall capacity factor of the PEC system with redox couples or redox carriers that separate HER and OER spatially and temporally to achieve H_2 production at night. PEC systems that produces H_2 and O_2 in two steps would share many system-level considerations with STCH systems.[47,48] For STCH, the reoxidation reactor and the reduction reactor can (but do not necessarily) operate at different rates, even in a continuous cycle. Furthermore, it is possible to store the reduced metal oxide (containing the oxygen vacancies) and reoxidize when the sun is not shining; however, doing so has implications for the heat integration and the metal oxide inventory in the design of the system, thus having efficiency and cost implications. Nevertheless, the capacity factor for STCH is constrained by the minimum annual DNI needed to build a cost-effective plant (desirable to have 6.5 kWh/m^2/day, but it will come down to the economics) and maximum storage capacity. Note that although a capacity factor of 100% is potentially achievable, the cost of the redox-active material and the insulation of the storage will likely be limiting and will determine viability.

CHALLENGES AND OUTLOOKS

Sustainable "green" hydrogen generation will be a crucial element for deep global decarbonization across multiple sectors in society. Low-temperature electrolysis (LTE) using alkaline (AEM) and proton exchange membrane (PEM) electrolyzers has recently received renewed interest in many countries; the largest alkaline electrolysis system was deployed in Aswan Dam at a capacity of 165 MW in the 1960s. While the direct solar-to-hydrogen technology pathways, including PEC and STCH, have a significantly lower technical readiness level (TRL) based on the demonstrated scale as well as the longevity of the demonstrated systems, there are unique aspects of these pathways when compared to LTE.[1] For example, direct solar-to-hydrogen pathways can be advantageous in locations without reliable electrical grid infrastructures, as they can avoid electrical transmission lines and losses. For PEC water-splitting, the largest photoactive area demonstrated to date was ∼1 m^2, in which the highest hydrogen production rate of ∼0.65 g/day and STH conversion efficiency of 0.4% were achieved with a fixed Al-doped $SrTiO_3$ photocatalyst system.[51] Highly efficient PEC devices that incorporate legacy PV materials, such as Si and III−V semiconductors, exhibited STH conversion efficiency >10% and longevity of the device from tens to hundreds of hours of operation.[95−98] For STCH, the largest demonstration facility is in the range of 750 kW, which had three fixed-bed reactors, with two containing $NiFe_2O_4$ and one with CeO_2 as redox-active materials;[99] no efficiency has been reported for that demonstration. Experimentally, the maximum efficiency reported for a thermochemical cycle has been 5.25% in a 4.1 kW fixed-bed reactor with CeO_2 operated in a solar simulator.[100] Among the redox-active materials for two-step STCH water-splitting, only ferrites and CeO_2-based materials have been demonstrated on a pilot scale,[101] and only CeO_2 has shown excellent cyclability and longevity with hundreds of cycles.[102]

> "While the direct solar-to-hydrogen technology pathways have a significantly lower technical readiness level based on the demonstrated scale as well as the longevity of the demonstrated systems, there are unique aspects of these pathways when compared to low-temperature electrolysis."

In a PEC system, the discovery of durable, cost-effective, and efficient photoelectrodes remains the top challenge for this technology. Despite approaching 20% STH conversion

https://doi.org/10.1021/acsenergylett.1c00758
ACS Energy Lett. 2021, 6, 3096−3113

efficiency, the stability of the state-of-the-art III−V tandem-based device still remains a limitation. Protecting the high-efficiency photoelectrodes that use traditional PV materials from corrosion in water-splitting conditions,[14,17,96,103,104] and discovering new PEC-unique photocathodes or photoanodes with semiconductor/electrolyte junctions, are two strategic approaches to improve the performance of the photoelectrodes.[10,11,90] A portfolio of materials are available for efficient and relatively stable operation of OER and HER in all pH regions. Notably, Earth-abundant, mixed-metal oxides, such as $NiFeO_x$, are often good candidates for OER, and mixed metals, such as NiMo, are often good candidates for HER in alkaline conditions.[90,105−108] However, discovery of efficient and stable OER catalysts with Earth-abundant materials in acidic conditions is not yet in hand.[109] One unique requirement for optimal catalysts for PEC water-splitting is the optical transparency of the catalyst to facilitate efficient light collection; various strategies that optimize the light path at the electrolyte/catalyst/semiconductor interfaces can further boost the device efficiency and expand the materials selections.[110−116] In addition, little is known about dynamic operations (diurnal cycles and bad weather days) and their impact on catalyst materials, which would be necessary to understand for real-world operation. For PEC devices, recent demonstrations of unassisted PEC water-splitting with various configurations exist, with STH conversion efficiencies that exceed 10% and device stability in the range of tens to hundreds of hours.[95−98] However, significant challenges remain in bringing the current PEC scale (typically <0.01 g/day) to the bench scale (0.1 kg/day) or subscale (2 kg/day).[72,73] In addition, standardization of device architectures and benchmarking conditions are important to meaningfully compare results and performances across different PEC materials from the research community.[117] Developing long-term stability protocols and corrosion analysis at the component level and at the device level also remains top priorities for the PEC community for the near future.

For STCH systems, the discovery of a new redox-active material able to reduce the solar input requirements per mole of H_2 produced while preserving good water-splitting thermodynamic and kinetic attributes is the top challenge for this technology. Furthermore, this ideal redox-active material should show fast redox kinetics, high cyclability, high thermal stress resistance, high thermal and oxygen ion conductivity, and low cost.[118] Currently, researchers in the field consider ceria the state-of-the-art, as it is the most investigated material and it exhibits very good reoxidation properties, excellent high-temperature stability, excellent cyclability, very good conductivities, and fast kinetics.[100,119] However, ceria is too difficult to reduce, pushing the reduction temperature up to 1500 °C or higher, or requiring a very low O_2 partial pressure (e.g., very high sweep flows) to obtain an appreciable reduction extent under inert gas sweeping.[38,40] On the other side, ceria is very easily reoxidized, allowing high H_2O/H_2 conversion (>10%) at high reoxidation temperatures (>1000 °C). A material like ceria with lower reduction enthalpy change (e.g., 15% lower) and similar reduction entropy change or slightly lower would reduce more easily while preserving the adequate reoxidation thermodynamics and kinetics. However, keeping the solid-state entropy change in reduction similar to that with ceria while reducing the enthalpy change may or may not be possible.[120] Next best will be to tune the enthalpy of reduction and maintain a significant solid-state entropy change.

Considering the STCH system design, the reduction of heat losses and heat requirements to the auxiliary systems would increase the overall system efficiency to approach theoretical values.[79,121] An efficient heat recovery system is necessary to optimally select the temperature difference between the reduction reaction (O_2 production) and the reoxidation reaction (H_2 production) without adversely affecting the STH conversion efficiency and taking advantage of a higher reduction extent and higher water conversion yield (i.e., limiting the amount of excess steam). Developing an effective (cost and performance) solid−solid heat exchange is a challenging endeavor, and no one has yet demonstrated 80% effectiveness.[57,59,60,122] Removing oxygen from the reduction reactor is the other auxiliary system technology receiving more attention, although not enough attention for real-world applications. Technological approaches to achieve the necessary low oxygen partial pressures must be energetically efficient and economically affordable. Currently, a second law efficiency of 10% in $N_2−O_2$ separation is considered acceptable in electrically driven devices. The development of thermally driven oxygen adsorption/desorption cycles could increase the STH conversion efficiency by using internal and low-quality process heat.[80] Although less studied, the H_2/H_2O separation process is also critical to achieve a high STH conversion efficiency. An ideal H_2/H_2O separation process would reuse the residual process heat from the reoxidation reactor and separate both substances in the gas phase, preventing the water phase change, as recovering the latent heat is typically a greater challenge than achieving high effectiveness gas−gas heat exchange, since >90% effectiveness for gas-phase recovery at high temperature has been reported in the literature.[123−126] More generally, finding optimal operating conditions or the ideal discoverable material does not enjoy consensus in the field.

Due to the high solar fluxes and high temperatures, in STCH, the receiver/reduction reactor is one of the most risky and critical components of the plant. It should be fabricated with materials resistant to severe thermal shocks and be able to work under high-temperature and oxidizing environments, noting that the materials are releasing oxygen inside of the reduction reactor. Nevertheless, the materials, the reactors, the heat exchange and heat integration, and the separations each face challenges for the approach to achieve its potential. Most of the focus has been on finding a material that is as good as ceria where ceria excels, and better than ceria where ceria falls short (namely striking the optimal balance between difficulty to reduce and difficulty to reoxidize). The reoxidation reactor is less risky than the reduction reactor from the point of view of materials, as its operating conditions are milder. However, it is just as critical. The heat captured in reoxidation plays an essential role in the STH conversion efficiency, as it can be reused to drive all the auxiliary processes of the plant. Currently, no reactor design has this feature developed.

"Both photoelectrochemical and solar thermochemical water-splitting systems can be extended to other reactions, such as CO_2 reduction and N_2 reduction."

https://doi.org/10.1021/acsenergylett.1c00758
ACS Energy Lett. 2021, 6, 3096−3113

Both PEC and STCH water-splitting systems can be extended to other reactions, such as CO_2 reduction and N_2 reduction. For PEC systems, CO_2 reduction and N_2 reduction share the same common half-reaction, e.g., oxygen evolution reaction (OER) to provide the needed protons for the reduction reactions.[127,128] However, due to the low solubility of CO_2 and N_2 in aqueous solutions, the PEC device architecture for CO_2 reduction and N_2 reduction can be very different from water-splitting reactions. For example, gas diffusion electrodes, which can relax the mass transport constraints, might be used in these devices.[129,130] In addition, polymeric membranes, such as Nafion, which can readily prevent the product crossovers for H_2 and O_2, would face additional challenges for liquid product separations in PEC CO_2 reduction systems.[131] For STCH systems, the cycles based on redox-active metal oxides directly apply to CO_2 splitting and/or combined CO_2/H_2O splitting for CO/syngas production, respectively.[40] Since the reaction Gibbs free energy of the CO_2 splitting is lower than that of the water-splitting at high temperatures, these cycles are less energy-demanding than the water-splitting. Other applications of STCH systems include oxygen pumping,[94] inert gas purification,[94] and N_2 production from air[132] and take advantage of the oxygen affinity from the reduced (oxygen-deficient) metal oxide. The STCH principles extend to redox-active metal nitrites, which can release nitrogen from their structure to react with H_2 and synthesize ammonia.[133]

In summary, we have compared and evaluated two direct solar hydrogen production approaches, e.g., PEC and STCH, in terms of sunlight utilization, device architecture and reactor design, STH conversion efficiency, and operating conditions of each system. Direct solar hydrogen production, while not cost-competitive with nearer-term approaches using renewable electrons, such as LTE, can be a unique alternative and complementary approach in certain regions of the world where the electricity grid is not fully deployed. It can also provide more energy resilience solutions to long-term energy storage and has the potential to achieve low-cost hydrogen production.

■ ASSOCIATED CONTENT

Supporting Information

The Supporting Information is available free of charge at https://pubs.acs.org/doi/10.1021/acsenergylett.1c00758.

Details of the quantification and parameters for loss analysis for PEC and STCH; examples of more realistic/less-optimistic cases for PEC and STCH (PDF)

■ AUTHOR INFORMATION

Corresponding Authors

Ellen B. Stechel − *ASU LightWorks® and School of Molecular Sciences, Arizona State University, Tempe, Arizona 85287-5402, United States;* orcid.org/0000-0002-5379-2908; Email: ellen.stechel@asu.edu

Chengxiang Xiang − *Liquid Sunlight Alliance (LiSA), and Department of Applied Physics and Material Science, California Institute of Technology, Pasadena, California 91125, United States;* orcid.org/0000-0002-1698-6754; Email: cxx@caltech.edu

Authors

Wen-Hui Cheng − *Department of Materials Science and Technology, National Cheng Kung University, Tainan 701, Taiwan; Liquid Sunlight Alliance (LiSA), and Department of Applied Physics and Material Science, California Institute of Technology, Pasadena, California 91125, United States;* orcid.org/0000-0003-3233-4606

Alberto de la Calle − *ASU LightWorks®, Arizona State University, Tempe, Arizona 85287-5402, United States*

Harry A. Atwater − *Liquid Sunlight Alliance (LiSA), and Department of Applied Physics and Material Science, California Institute of Technology, Pasadena, California 91125, United States;* orcid.org/0000-0001-9435-0201

Complete contact information is available at: https://pubs.acs.org/10.1021/acsenergylett.1c00758

Author Contributions

†Wen-Hui Cheng and Alberto de la Calle contributed equally to this work.

Notes

The authors declare no competing financial interest.

Biographies

Wen-Hui Cheng is Assistant Professor at National Cheng Kung University, Taiwan. She received her Ph.D. from California Institute of Technology in Materials Science and conducted postdoctoral research at Stanford University. Her research interests include manipulating light to assist chemistry for energy application and engineering structure for optoelectronics.

Website: https://sophiasophia0701.wixsite.com/clpo

Alberto de la Calle is Assistant Research Scientist at Arizona State University. He performed his Ph.D. at Plataforma Solar de Almeria, Spain and conducted postdoctoral research at CSIRO Energy, Australia. His research interests include concentrating solar thermal technologies, thermal energy storage, thermochemical cycles for fuel production and renewable ammonia.

Website: https://sustainability-innovation.asu.edu/lightworks/person/alberto-de-la-calle/

Harry Atwater is the Howard Hughes Professor of Applied Physics and Materials Science at Caltech and the Director of the Liquid Sunlight Alliance. His scientific interests span light-matter interactions from quantum nanophotonics, two-dimensional materials and metasurfaces to solar photovoltaics and artificial photosynthesis. He is an early pioneer in nanophotonics and plasmonics who names the field.

Website: https://daedalus.caltech.edu

Ellen B. Stechel is Co-Director of ASU LightWorks® and Professor of Practice in School of Molecular Sciences at Arizona State University. Her current research focuses on materials and systems design for solar technologies for producing sustainable fuels from advanced water-splitting, clean water, renewable ammonia, and for thermochemical and chemical energy storage.

Website: https://sustainability-innovation.asu.edu/lightworks/person/ellen-stechel/

Chengxiang Xiang is Research Professor of Applied Physics and Materials Science at California Institute of Technology. His research interests include design and fabrication of high efficiency solar-fuel prototypes, optoelectronic-catalytic modeling of advanced photo-electrochemical systems, multi-ion transport modeling in solution and polymer electrolytes and electrochemical CO_2 capture from dilute sources.

Website: https://cxx.caltech.edu

■ ACKNOWLEDGMENTS

W.-H.C. acknowledges the support from Ministry of Science and Technology (2030 Cross-Generation Young Scholars Program), Taiwan and Ministry of Education (Yushan Scholar Program), Taiwan. The authors acknowledge the support from the Fuel Cell Technologies Office, of the U.S. Department of Energy, Energy Efficiency and Renewable Energy under contract number DE-EE0008092. The PEC analysis was partly based on work performed by the Liquid Sunlight Alliance, which is supported by the U.S. Department of Energy, Office of Science, Office of Basic Energy Sciences, Fuels from Sunlight Hub under Award Number DE-SC0021266. This material is also partially based on work supported by the U.S. Department of Energy, Energy Efficiency and Renewable Energy (EERE) Solar Energy Technologies Office (SETO) under Award No. DE−EE0008991.

■ REFERENCES

(1) Ardo, S.; Fernandez Rivas, D.; Modestino, M. A.; Schulze Greiving, V.; Abdi, F. F.; Alarcon Llado, E.; Artero, V.; Ayers, K.; Battaglia, C.; Becker, J. P.; Bederak, D.; Berger, A.; Buda, F.; Chinello, E.; Dam, B.; Di Palma, V.; Edvinsson, T.; Fujii, K.; Gardeniers, H.; Geerlings, H.; Hashemi, S. M.; Haussener, S.; Houle, F.; Huskens, J.; James, B. D.; Konrad, K.; Kudo, A.; Kunturu, P. P.; Lohse, D.; Mei, B.; Miller, E. L.; Moore, G. F.; Muller, J.; Orchard, K. L.; Rosser, T. E.; Saadi, F. H.; Schüttauf, J. W.; Seger, B.; Sheehan, S. W.; Smith, W. A.; Spurgeon, J.; Tang, M. H.; Van De Krol, R.; Vesborg, P. C. K.; Westerik, P. Pathways to Electrochemical Solar-Hydrogen Technologies. *Energy Environ. Sci.* **2018**, *11* (10), 2768−2783.

(2) Herron, J. A.; Kim, J.; Upadhye, A. A.; Huber, G. W.; Maravelias, C. T. A General Framework for the Assessment of Solar Fuel Technologies. *Energy Environ. Sci.* **2015**, *8* (1), 126−157.

(3) Tuller, H. L. Solar to Fuels Conversion Technologies: A Perspective. *Mater. Renew. Sustain. Energy* **2017**, *6* (1), 1−16.

(4) Pinaud, B. A.; Benck, J. D.; Seitz, L. C.; Forman, A. J.; Chen, Z.; Deutsch, T. G.; James, B. D.; Baum, K. N.; Baum, G. N.; Ardo, S.; Wang, H.; Miller, E.; Jaramillo, T. F. Technical and Economic Feasibility of Centralized Facilities for Solar Hydrogen Production via Photocatalysis and Photoelectrochemistry. *Energy Environ. Sci.* **2013**, *6* (7), 1983−2002.

(5) Hisatomi, T.; Domen, K. Reaction Systems for Solar Hydrogen Production via Water Splitting with Particulate Semiconductor Photocatalysts. *Nat. Catal.* **2019**, *2* (5), 387−399.

(6) Hinkley, J.; Hayward, J.; McNaughton, R.; Edwards, J.; Lovegrove, K. *Concentrating Solar Fuels Roadmap: Final Report Towards Sustainable Energy ARENA Project Solar Hybrid Fuels (3-A018)*. 2016.

(7) Budama, V. K.; Johnson, N. G.; McDaniel, A.; Ermanoski, I.; Stechel, E. B. Thermodynamic Development and Design of a Concentrating Solar Thermochemical Water-Splitting Process for Co-Production of Hydrogen and Electricity. *Int. J. Hydrogen Energy* **2018**, *43* (37), 17574−17587.

(8) Bae, D.; Pedersen, T.; Seger, B.; Iandolo, B.; Hansen, O.; Vesborg, P. C. K.; Chorkendorff, I. Carrier-Selective p- and n-Contacts for Efficient and Stable Photocatalytic Water Reduction. *Catal. Today* **2017**, *290*, 59−64.

(9) Walter, M. G.; Warren, E. L.; McKone, J. R.; Boettcher, S. W.; Mi, Q.; Santori, E. A.; Lewis, N. S. Solar Water Splitting Cells. *Chem. Rev.* **2010**, *110* (11), 6446−6473.

(10) Qiu, Y.; Liu, W.; Chen, W.; Zhou, G.; Hsu, P. C.; Zhang, R.; Liang, Z.; Fan, S.; Zhang, Y.; Cui, Y. Efficient Solar-Driven Water Splitting by Nanocone $BiVO_4$-Perovskite Tandem Cells. *Sci. Adv.* **2016**, *2* (6), No. e1501764.

(11) Huang, D.; Wang, K.; Yu, L.; Nguyen, T. H.; Ikeda, S.; Jiang, F. Over 1% Efficient Unbiased Stable Solar Water Splitting Based on a Sprayed Cu_2ZnSnS_4 Photocathode Protected by a HfO_2 Photocorrosion-Resistant Film. *ACS Energy Lett.* **2018**, *3* (8), 1875−1881.

(12) Tan, M. X.; Laibinis, P. E.; Nguyen, S. T.; Kesselman, J. M.; Stanton, C. E.; Lewis, N. S. Principles and Applications of Semiconductor Photoelectrochemistry. *Prog. Inorg. Chem.* **2007**, *41*, 21−144.

(13) Khaselev, O.; Turner, J. A. A Monolithic Photovoltaic-Photoelectrochemical Device for Hydrogen Production via Water Splitting. *Science* **1998**, *280* (5362), 425−427.

(14) Cheng, W. H.; Richter, M. H.; May, M. M.; Ohlmann, J.; Lackner, D.; Dimroth, F.; Hannappel, T.; Atwater, H. A.; Lewerenz, H. J. Monolithic Photoelectrochemical Device for Direct Water Splitting with 19% Efficiency. *ACS Energy Lett.* **2018**, *3* (8), 1795−1800.

(15) Reece, S. Y.; Hamel, J. A.; Sung, K.; Jarvi, T. D.; Esswein, A. J.; Pijpers, J. J. H.; Nocera, D. G. Wireless Solar Water Splitting Using Silicon-Based Semiconductors and Earth-Abundant Catalysts. *Science* **2011**, *334* (6056), 645−648.

(16) Young, J. L.; Steiner, M. A.; Döscher, H.; France, R. M.; Turner, J. A.; Deutsch, T. G. Direct Solar-to-Hydrogen Conversion via Inverted Metamorphic Multi-Junction Semiconductor Architectures. *Nat. Energy* **2017**, *2* (4), 17028.

(17) Verlage, E.; Hu, S.; Liu, R.; Jones, R. J. R.; Sun, K.; Xiang, C.; Lewis, N. S.; Atwater, H. A. A Monolithically Integrated, Intrinsically Safe, 10% Efficient, Solar-Driven Water-Splitting System Based on Active, Stable Earth-Abundant Electrocatalysts in Conjunction with Tandem III−V Light Absorbers Protected by Amorphous TiO_2 Films. *Energy Environ. Sci.* **2015**, *8* (11), 3166−3172.

(18) May, M. M.; Lewerenz, H.-J.; Lackner, D.; Dimroth, F.; Hannappel, T. Efficient Direct Solar-to-Hydrogen Conversion by in Situ Interface Transformation of a Tandem Structure. *Nat. Commun.* **2015**, *6* (1), 8286.

(19) Steinfeld, A. Solar Thermochemical Production of Hydrogen−a Review. *Sol. Energy* **2005**, *78* (5), 603−615.

(20) Agrafiotis, C.; Roeb, M.; Sattler, C. A Review on Solar Thermal Syngas Production via Redox Pair-Based Water/Carbon Dioxide Splitting Thermochemical Cycles. *Renewable Sustainable Energy Rev.* **2015**, *42*, 254−285.

(21) Funk, J. E. Thermochemical Hydrogen Production: Past and Present. *Int. J. Hydrogen Energy* **2001**, *26* (3), 185−190.

(22) Loutzenhiser, P. G.; Steinfeld, A. Solar Syngas Production from CO_2 and H_2O in a Two-Step Thermochemical Cycle via Zn/ZnO Redox Reactions: Thermodynamic Cycle Analysis. *Int. J. Hydrogen Energy* **2011**, *36* (19), 12141−12147.

(23) Steinfeld, A. Solar Hydrogen Production via a Two-Step Water-Splitting Thermochemical Cycle Based on Zn/ZnO Redox Reactions. *Int. J. Hydrogen Energy* **2002**, *27* (6), 611−619.

(24) Koepf, E.; Villasmil, W.; Meier, A. Pilot-Scale Solar Reactor Operation and Characterization for Fuel Production via the Zn/ZnO Thermochemical Cycle. *Appl. Energy* **2016**, *165*, 1004−1023.

(25) Abanades, S.; Charvin, P.; Lemont, F.; Flamant, G. Novel Two-Step SnO_2/SnO Water-Splitting Cycle for Solar Thermochemical Production of Hydrogen. *Int. J. Hydrogen Energy* **2008**, *33* (21), 6021−6030.

(26) Nakamura, T. Hydrogen Production from Water Utilizing Solar Heat at High Temperatures. *Sol. Energy* **1977**, *19* (5), 467−475.

(27) Charvin, P.; Abanades, S.; Flamant, G.; Lemort, F. Two-Step Water Splitting Thermochemical Cycle Based on Iron Oxide Redox Pair for Solar Hydrogen Production. *Energy* **2007**, *32* (7), 1124−1133.

(28) Scheffe, J. R.; Li, J.; Weimer, A. W. A Spinel Ferrite/Hercynite Water-Splitting Redox Cycle. *Int. J. Hydrogen Energy* **2010**, *35* (8), 3333−3340.

(29) Roeb, M.; Säck, J. P.; Rietbrock, P.; Prahl, C.; Schreiber, H.; Neises, M.; de Oliveira, L.; Graf, D.; Ebert, M.; Reinalter, W.; Meyer-Grünefeldt, M.; Sattler, C.; Lopez, A.; Vidal, A.; Elsberg, A.; Stobbe, P.; Jones, D.; Steele, A.; Lorentzou, S.; Pagkoura, C.; Zygogianni, A.; Agrafiotis, C.; Konstandopoulos, A. G. Test Operation of a 100kW Pilot Plant for Solar Hydrogen Production from Water on a Solar Tower. *Sol. Energy* **2011**, *85* (4), 634−644.

https://doi.org/10.1021/acsenergylett.1c00758
ACS Energy Lett. 2021, 6, 3096−3113

(30) Miller, J. E.; McDaniel, A. H.; Allendorf, M. D. Considerations in the Design of Materials for Solar-Driven Fuel Production Using Metal-Oxide Thermochemical Cycles. *Adv. Energy Mater.* **2014**, *4* (2), 1300469.
(31) Kaur, H.; Wang, M.; Gorensek, M. B.; Chen, C. C. Thermodynamic Modeling of the Hybrid Sulfur (HyS) Cycle for Hydrogen Production. *Fluid Phase Equilib.* **2018**, *460*, 175−188.
(32) Sattler, C.; Roeb, M.; Agrafiotis, C.; Thomey, D. Solar Hydrogen Production via Sulphur Based Thermochemical Water-Splitting. *Sol. Energy* **2017**, *156*, 30−47.
(33) Gorensek, M. B.; Corgnale, C.; Summers, W. A. Development of the Hybrid Sulfur Cycle for Use with Concentrated Solar Heat. I. Conceptual Design. *Int. J. Hydrogen Energy* **2017**, *42* (33), 20939−20954.
(34) Xu, B.; Bhawe, Y.; Davis, M. E. Low-Temperature, Manganese Oxide-Based, Thermochemical Water Splitting Cycle. *Proc. Natl. Acad. Sci. U. S. A.* **2012**, *109* (24), 9260−9264.
(35) Bayón, A.; De La Peña O'Shea, V. A.; Coronado, J. M.; Serrano, D. P. Role of the Physicochemical Properties of Hausmannite on the Hydrogen Production via the Mn_3O_4-NaOH Thermochemical Cycle. *Int. J. Hydrogen Energy* **2016**, *41* (1), 113−122.
(36) Bayón, A.; De La PenãO'Shea, V. A.; Serrano, D. P.; Coronado, J. M. Exploring the Alternative MnO-Na_2CO_3thermochemical Cycle for Water Splitting. *J. CO_2 Util.* **2020**, *42*, 101264.
(37) ABANADES. Metal Oxides Applied to Thermochemical Water-Splitting for Hydrogen Production Using Concentrated Solar Energy. *ChemEngineering* **2019**, *3* (3), 63. .
(38) Muhich, C.; Steinfeld, A. Principles of Doping Ceria for the Solar Thermochemical Redox Splitting of H_2O and CO_2. *J. Mater. Chem. A* **2017**, *5* (30), 15578−15590.
(39) Bhosale, R. R.; Takalkar, G.; Sutar, P.; Kumar, A.; AlMomani, F.; Khraisheh, M. A Decade of Ceria Based Solar Thermochemical H_2O/CO_2 Splitting Cycle. *Int. J. Hydrogen Energy* **2019**, *44* (1), 34−60.
(40) Lu, Y.; Zhu, L.; Agrafiotis, C.; Vieten, J.; Roeb, M.; Sattler, C. Solar Fuels Production: Two-Step Thermochemical Cycles with Cerium-Based Oxides. *Prog. Energy Combust. Sci.* **2019**, *75*, 100785.
(41) Chueh, W. C.; Haile, S. M. A Thermochemical Study of Ceria: Exploiting an Old Material for New Modes of Energy Conversion and CO_2 Mitigation. *Philos. Trans. R. Soc., A* **2010**, *368* (1923), 3269−3294.
(42) Bayon, A.; de la Calle, A.; Ghose, K. K.; Page, A.; McNaughton, R. Experimental, Computational and Thermodynamic Studies in Perovskites Metal Oxides for Thermochemical Fuel Production: A Review. *Int. J. Hydrogen Energy* **2020**, *45* (23), 12653−12679.
(43) Kubicek, M.; Bork, A. H.; Rupp, J. L. M. Perovskite Oxides-a Review on a Versatile Material Class for Solar-to-Fuel Conversion Processes. *J. Mater. Chem. A* **2017**, *5* (24), 11983−12000.
(44) Haeussler, A.; Abanades, S.; Jouannaux, J.; Julbe, A. Non-Stoichiometric Redox Active Perovskite Materials for Solar Thermochemical Fuel Production: A Review. *Catalysts* **2018**, *8* (12), 611.
(45) Bayon, A.; Calle de la, A.; Stechel, E. B.; Muhich, C. Operational Limits of Redox Metal Oxides Performing Thermochemical Water Splitting. *Energy Technol.* **2021**, 2100222.
(46) Ager, J. W.; Shaner, M. R.; Walczak, K. A.; Sharp, I. D.; Ardo, S. Experimental Demonstrations of Spontaneous, Solar-Driven Photoelectrochemical Water Splitting. *Energy Environ. Sci.* **2015**, *8* (10), 2811−2824.
(47) Landman, A.; Dotan, H.; Shter, G. E.; Wullenkord, M.; Houaijia, A.; Maljusch, A.; Grader, G. S.; Rothschild, A. Photoelectrochemical Water Splitting in Separate Oxygen and Hydrogen Cells. *Nat. Mater.* **2017**, *16* (6), 646−651.
(48) Qi, Y.; Zhao, Y.; Gao, Y.; Li, D.; Li, Z.; Zhang, F.; Li, C. Redox-Based Visible-Light-Driven Z-Scheme Overall Water Splitting with Apparent Quantum Efficiency Exceeding 10%. *Joule* **2018**, *2* (11), 2393−2402.
(49) Kim, J. H.; Hansora, D.; Sharma, P.; Jang, J. W.; Lee, J. S. Toward Practical Solar Hydrogen Production-an Artificial Photosynthetic Leaf-to-Farm Challenge. *Chem. Soc. Rev.* **2019**, *48* (7), 1908−1971.
(50) Hisatomi, T.; Domen, K. Introductory Lecture: Sunlight-Driven Water Splitting and Carbon Dioxide Reduction by Heterogeneous Semiconductor Systems as Key Processes in Artificial Photosynthesis. *Faraday Discuss.* **2017**, *198* (0), 11−35.
(51) Goto, Y.; Hisatomi, T.; Wang, Q.; Higashi, T.; Ishikiriyama, K.; Maeda, T.; Sakata, Y.; Okunaka, S.; Tokudome, H.; Katayama, M.; Akiyama, S.; Nishiyama, H.; Inoue, Y.; Takewaki, T.; Setoyama, T.; Minegishi, T.; Takata, T.; Yamada, T.; Domen, K. A Particulate Photocatalyst Water-Splitting Panel for Large-Scale Solar Hydrogen Generation. *Joule* **2018**, *2* (3), 509−520.
(52) Liu, J.; Liu, Y.; Liu, N.; Han, Y.; Zhang, X.; Huang, H.; Lifshitz, Y.; Lee, S.-T.; Zhong, J.; Kang, Z. Metal-Free Efficient Photocatalyst for Stable Visible Water Splitting via a Two-Electron Pathway. *Science* **2015**, *347* (6225), 970−974.
(53) Liu, X.-Y.; Chen, H.; Wang, R.; Shang, Y.; Zhang, Q.; Li, W.; Zhang, G.; Su, J.; Dinh, C. T.; de Arquer, F. P. G.; Li, J.; Jiang, J.; Mi, Q.; Si, R.; Li, X.; Sun, Y.; Long, Y.-T.; Tian, H.; Sargent, E. H.; Ning, Z. 0D-2D Quantum Dot: Metal Dichalcogenide Nanocomposite Photocatalyst Achieves Efficient Hydrogen Generation. *Adv. Mater.* **2017**, *29* (22), 1605646.
(54) Tembhurne, S.; Nandjou, F.; Haussener, S. A Thermally Synergistic Photo-Electrochemical Hydrogen Generator Operating under Concentrated Solar Irradiation. *Nat. Energy* **2019**, *4* (5), 399−407.
(55) de la Calle, A.; Roca, L.; Yebra, L. J.; Dormido, S. Modeling of a Two-Step Solar Hydrogen Production Plant. *Int. J. Hydrogen Energy* **2012**, *37* (14), 10549−10556.
(56) Brendelberger, S.; Rosenstiel, A.; Lopez-Roman, A.; Prieto, C.; Sattler, C. Performance Analysis of Operational Strategies for Monolithic Receiver-Reactor Arrays in Solar Thermochemical Hydrogen Production Plants. *Int. J. Hydrogen Energy* **2020**, *45* (49), 26104−26116.
(57) Ermanoski, I.; Siegel, N. P.; Stechel, E. B. A New Reactor Concept for Efficient Solar-Thermochemical Fuel Production. *J. Sol. Energy Eng.* **2013**, *135* (3). DOI: 10.1115/1.4023356.
(58) Kodama, T.; Bellan, S.; Gokon, N.; Cho, H. S. Particle Reactors for Solar Thermochemical Processes. *Sol. Energy* **2017**, *156*, 113−132.
(59) Diver, R. B.; Miller, J. E.; Allendorf, M. D.; Siegel, N. P.; Hogan, R. E. Solar Thermochemical Water-Splitting Ferrite-Cycle Heat Engines. *J. Sol. Energy Eng.* **2008**, *130* (4), 0410011−0410018.
(60) Lapp, J.; Davidson, J. H.; Lipiński, W. Heat Transfer Analysis of a Solid-Solid Heat Recuperation System for Solar-Driven Non-stoichiometric Redox Cycles. *J. Sol. Energy Eng.* **2013**, *135* (3). DOI: 10.1115/1.4023357.
(61) de la Calle, A.; Bayon, A. Annual Performance of a Thermochemical Solar Syngas Production Plant Based on Non-Stoichiometric CeO_2. *Int. J. Hydrogen Energy* **2019**, *44* (3), 1409−1424.
(62) Chen, Y.; Sun, K.; Audesirk, H.; Xiang, C.; Lewis, N. S. A Quantitative Analysis of the Efficiency of Solar-Driven Water-Splitting Device Designs Based on Tandem Photoabsorbers Patterned with Islands of Metallic Electrocatalysts. *Energy Environ. Sci.* **2015**, *8* (6), 1736−1747.
(63) Rodriguez, C. A.; Modestino, M. A.; Psaltis, D.; Moser, C. Design and Cost Considerations for Practical Solar-Hydrogen Generators. *Energy Environ. Sci.* **2014**, *7* (12), 3828−3835.
(64) Roger, I.; Shipman, M. A.; Symes, M. D. Earth-Abundant Catalysts for Electrochemical and Photoelectrochemical Water Splitting. *Nat. Rev. Chem.* **2017**, *1* (1), 1−13.
(65) Simbolotti, G. *Concentrating Solar Power Technology Brief*. IEA-ETSAP and IRENA 2013.
(66) Stechel, E. B.; Miller, J. E. Re-Energizing CO_2 to Fuels with the Sun: Issues of Efficiency, Scale, and Economics. *J. CO_2 Util.* **2013**, *1*, 28−36.
(67) Ong, S.; Campbell, C.; Denholm, P.; Margolis, R.; Heath, G. *Land-Use Requirements for Solar Power Plants in the United States*;

National Renewable Energy Lab.(NREL), Golden, CO (United States), 2013.
(68) Siegel, N. P.; Miller, J. E.; Ermanoski, I.; Diver, R. B.; Stechel, E. B. Factors Affecting the Efficiency of Solar Driven Metal Oxide Thermochemical Cycles. *Ind. Eng. Chem. Res.* **2013**, *52* (9), 3276−3286.
(69) Shaner, M. R.; Atwater, H. A.; Lewis, N. S.; McFarland, E. W. A Comparative Technoeconomic Analysis of Renewable Hydrogen Production Using Solar Energy. *Energy Environ. Sci.* **2016**, *9* (7), 2354−2371.
(70) Jensen, J. O.; Vestbø, A. P.; Li, Q.; Bjerrum, N. J. The Energy Efficiency of Onboard Hydrogen Storage. *J. Alloys Compd.* **2007**, *446*−*447*, 723−728.
(71) Standard state and enthalpy of formation, Gibbs free energy of formation, entropy and heat capacity https://www.engineeringtoolbox.com/standard-state-enthalpy-formation-definition-value-Gibbs-free-energy-entropy-molar-heat-capacity-d_1978.html (accessed Aug 5, 2020).
(72) Turan, B.; Becker, J. P.; Urbain, F.; Finger, F.; Rau, U.; Haas, S. Upscaling of Integrated Photoelectrochemical Water-Splitting Devices to Large Areas. *Nat. Commun.* **2016**, *7* (1), 1−9.
(73) Becker, J. P.; Turan, B.; Smirnov, V.; Welter, K.; Urbain, F.; Wolff, J.; Haas, S.; Finger, F. A Modular Device for Large Area Integrated Photoelectrochemical Water-Splitting as a Versatile Tool to Evaluate Photoabsorbers and Catalysts. *J. Mater. Chem. A* **2017**, *5* (10), 4818−4826.
(74) Chen, Y.; Hu, S.; Xiang, C.; Lewis, N. S. A Sensitivity Analysis to Assess the Relative Importance of Improvements in Electrocatalysts, Light Absorbers, and System Geometry on the Efficiency of Solar-Fuels Generators. *Energy Environ. Sci.* **2015**, *8* (3), 876−886.
(75) Perez-Rodriguez, P.; Vijselaar, W.; Huskens, J.; Stam, M.; Falkenberg, M.; Zeman, M.; Smith, W.; Smets, A. H. M. Designing a Hybrid Thin-Film/Wafer Silicon Triple Photovoltaic Junction for Solar Water Splitting. *Prog. Photovoltaics* **2019**, *27* (3), 245−254.
(76) Boretti, A. Technology Readiness Level of Solar Thermochemical Splitting Cycles. *ACS Energy Lett.* **2021**, 1170−1174.
(77) Zinkevich, M.; Djurovic, D.; Aldinger, F. Thermodynamic Modelling of the Cerium-Oxygen System. *Solid State Ionics* **2006**, *177* (11−12), 989−1001.
(78) Dähler, F.; Wild, M.; Schäppi, R.; Haueter, P.; Cooper, T.; Good, P.; Larrea, C.; Schmitz, M.; Furler, P.; Steinfeld, A. Optical Design and Experimental Characterization of a Solar Concentrating Dish System for Fuel Production via Thermochemical Redox Cycles. *Sol. Energy* **2018**, *170*, 568−575.
(79) Li, S.; Wheeler, V. M.; Kreider, P. B.; Bader, R.; Lipiński, W. Thermodynamic Analyses of Fuel Production via Solar-Driven Non-Stoichiometric Metal Oxide Redox Cycling. Part 2. Impact of Solid-Gas Flow Configurations and Active Material Composition on System-Level Efficiency. *Energy Fuels* **2018**, *32* (10), 10848−10863.
(80) Ermanoski, I.; Stechel, E. B. Thermally-Driven Adsorption/Desorption Cycle for Oxygen Pumping in Thermochemical Fuel Production. *Sol. Energy* **2020**, *198*, 578−585.
(81) de la Calle, A.; Bayon, A.; Pye, J. Techno-Economic Assessment of a High-Efficiency, Low-Cost Solar-Thermal Power System with Sodium Receiver, Phase-Change Material Storage, and Supercritical CO_2 Recompression Brayton Cycle. *Sol. Energy* **2020**, *199*, 885−900.
(82) Nelson, J.; Johnson, N. G.; Doron, P.; Stechel, E. B. Thermodynamic Modeling of Solarized Microturbine for Combined Heat and Power Applications. *Appl. Energy* **2018**, *212*, 592−606.
(83) Budama, V. K.; Johnson, N. G.; Ermanoski, I.; Stechel, E. B. Techno-Economic Analysis of Thermochemical Water-Splitting System for Co-Production of Hydrogen and Electricity. *Int. J. Hydrogen Energy* **2021**, *46* (2), 1656−1670.
(84) Singh, P.; Ravindra, N. M. Temperature Dependence of Solar Cell Performance - An Analysis. *Sol. Energy Mater. Sol. Cells* **2012**, *101*, 36−45.
(85) Siefer, G.; Bett, A. W. Analysis of Temperature Coefficients for III-V Multi-Junction Concentrator Cells. *Prog. Photovoltaics* **2014**, *22* (5), 515−524.
(86) Haussener, S.; Hu, S.; Xiang, C.; Weber, A. Z.; Lewis, N. S. Simulations of the Irradiation and Temperature Dependence of the Efficiency of Tandem Photoelectrochemical Water-Splitting Systems. *Energy Environ. Sci.* **2013**, *6* (12), 3605−3618.
(87) Carmo, M.; Fritz, D. L.; Mergel, J.; Stolten, D. A Comprehensive Review on PEM Water Electrolysis. *Int. J. Hydrogen Energy* **2013**, *38* (12), 4901−4934.
(88) McCrory, C. C. L.; Jung, S.; Ferrer, I. M.; Chatman, S. M.; Peters, J. C.; Jaramillo, T. F. Benchmarking Hydrogen Evolving Reaction and Oxygen Evolving Reaction Electrocatalysts for Solar Water Splitting Devices. *J. Am. Chem. Soc.* **2015**, *137* (13), 4347−4357.
(89) Park, J.; Yang, W.; Oh, Y.; Tan, J.; Lee, H.; Boppella, R.; Moon, J. Efficient Solar-to-Hydrogen Conversion from Neutral Electrolytes Using Morphology-Controlled Sb_2Se_3 Light Absorbers. *ACS Energy Lett.* **2019**, *4* (2), 517−526.
(90) Lee, S. A.; Lee, T. H.; Kim, C.; Lee, M. G.; Choi, M. J.; Park, H.; Choi, S.; Oh, J.; Jang, H. W. Tailored NiO_x/Ni Cocatalysts on Silicon for Highly Efficient Water Splitting Photoanodes via Pulsed Electrodeposition. *ACS Catal.* **2018**, *8* (8), 7261−7269.
(91) Ledezma-Yanez, I.; Wallace, W. D. Z.; Sebastián-Pascual, P.; Climent, V.; Feliu, J. M.; Koper, M. T. M. Interfacial Water Reorganization as a PH-Dependent Descriptor of the Hydrogen Evolution Rate on Platinum Electrodes. *Nat. Energy* **2017**, *2* (4), 17031.
(92) Singh, M. R.; Clark, E. L.; Bell, A. T. Effects of Electrolyte, Catalyst, and Membrane Composition and Operating Conditions on the Performance of Solar-Driven Electrochemical Reduction of Carbon Dioxide. *Phys. Chem. Chem. Phys.* **2015**, *17* (29), 18924−18936.
(93) Bulfin, B.; Call, F.; Lange, M.; Lübben, O.; Sattler, C.; Pitz-Paal, R.; Shvets, I. V. Thermodynamics of CeO_2 Thermochemical Fuel Production. *Energy Fuels* **2015**, *29* (2), 1001−1009.
(94) Brendelberger, S.; Vieten, J.; Roeb, M.; Sattler, C. Thermochemical Oxygen Pumping for Improved Hydrogen Production in Solar Redox Cycles. *Int. J. Hydrogen Energy* **2019**, *44* (20), 9802−9810.
(95) Bae, D.; Seger, B.; Vesborg, P. C. K.; Hansen, O.; Chorkendorff, I. Strategies for Stable Water Splitting via Protected Photoelectrodes. *Chem. Soc. Rev.* **2017**, *46* (7), 1933−1954.
(96) Ben-Naim, M.; Britto, R. J.; Aldridge, C. W.; Mow, R.; Steiner, M. A.; Nielander, A. C.; King, L. A.; Friedman, D. J.; Deutsch, T. G.; Young, J. L.; Jaramillo, T. F. Addressing the Stability Gap in Photoelectrochemistry: Molybdenum Disulfide Protective Catalysts for Tandem III−V Unassisted Solar Water Splitting. *ACS Energy Lett.* **2020**, *5*, 2631−2640.
(97) Kang, D.; Young, J. L.; Lim, H.; Klein, W. E.; Chen, H.; Xi, Y.; Gai, B.; Deutsch, T. G.; Yoon, J. Printed Assemblies of GaAs Photoelectrodes with Decoupled Optical and Reactive Interfaces for Unassisted Solar Water Splitting. *Nat. Energy* **2017**, *2* (5), 17043.
(98) Digdaya, I. A.; Adhyaksa, G. W. P.; Trześniewski, B. J.; Garnett, E. C.; Smith, W. A. Interfacial Engineering of Metal-Insulator-Semiconductor Junctions for Efficient and Stable Photoelectrochemical Water Oxidation. *Nat. Commun.* **2017**, *8* (1), 1−8.
(99) González-Pardo, A.; Denk, T.; Vidal, A. Lessons Learnt during the Construction and Start-up of 3 Cylindrical Cavity-Receivers Facility Integrated in a 750 KW Solar Tower Plant for Hydrogen Production. *AIP Conf. Proc.* **2019**, *2303* (1), 170008.
(100) Marxer, D.; Furler, P.; Takacs, M.; Steinfeld, A. Solar Thermochemical Splitting of CO_2 into Separate Streams of CO and O_2 with High Selectivity, Stability, Conversion, and Efficiency. *Energy Environ. Sci.* **2017**, *10* (5), 1142−1149.
(101) Yadav, D.; Banerjee, R. A Review of Solar Thermochemical Processes. *Renewable Sustainable Energy Rev.* **2016**, *54*, 497−532.
(102) Chueh, W. C.; Falter, C.; Abbott, M.; Scipio, D.; Furler, P.; Haile, S. M.; Steinfeld, A. High-Flux Solar-Driven Thermochemical Dissociation of CO_2 and H_2O Using Nonstoichiometric Ceria. *Science* **2010**, *330* (6012), 1797−1801.

(103) Gu, J.; Aguiar, J. A.; Ferrere, S.; Steirer, K. X.; Yan, Y.; Xiao, C.; Young, J. L.; Al-Jassim, M.; Neale, N. R.; Turner, J. A. A Graded Catalytic-Protective Layer for an Efficient and Stable Water-Splitting Photocathode. *Nat. Energy* **2017**, *2* (2), 1−8.
(104) Young, J. L.; Steiner, M. A.; Döscher, H.; France, R. M.; Turner, J. A.; Deutsch, T. G. Direct Solar-to-Hydrogen Conversion via Inverted Metamorphic Multi-Junction Semiconductor Architectures. *Nat. Energy* **2017**, *2* (4), 17028.
(105) Roger, I.; Shipman, M. A.; Symes, M. D. Earth-Abundant Catalysts for Electrochemical and Photoelectrochemical Water Splitting. *Nat. Rev. Chem.* **2017**, *1* (1), 1−13.
(106) Kuang, Y.; Kenney, M. J.; Meng, Y.; Hung, W. H.; Liu, Y.; Huang, J. E.; Prasanna, R.; Li, P.; Li, Y.; Wang, L.; Lin, M. C.; McGehee, M. D.; Sun, X.; Dai, H. Solar-Driven, Highly Sustained Splitting of Seawater into Hydrogen and Oxygen Fuels. *Proc. Natl. Acad. Sci. U. S. A.* **2019**, *116* (14), 6624−6629.
(107) Loget, G.; Fabre, B.; Fryars, S.; Mériadec, C.; Ababou-Girard, S. Dispersed Ni Nanoparticles Stabilize Silicon Photoanodes for Efficient and Inexpensive Sunlight-Assisted Water Oxidation. *ACS Energy Lett.* **2017**, *2* (3), 569−573.
(108) Sun, K.; Moreno-Hernandez, I. A.; Schmidt, W. C.; Zhou, X.; Crompton, J. C.; Liu, R.; Saadi, F. H.; Chen, Y.; Papadantonakis, K. M.; Lewis, N. S. A Comparison of the Chemical, Optical and Electrocatalytic Properties of Water-Oxidation Catalysts for Use in Integrated Solar-Fuel Generators. *Energy Environ. Sci.* **2017**, *10* (4), 987−1002.
(109) Zhou, L.; Shinde, A.; Montoya, J. H.; Singh, A.; Gul, S.; Yano, J.; Ye, Y.; Crumlin, E. J.; Richter, M. H.; Cooper, J. K.; Stein, H. S.; Haber, J. A.; Persson, K. A.; Gregoire, J. M. Rutile Alloys in the Mn-Sb-O System Stabilize Mn^{3+} to Enable Oxygen Evolution in Strong Acid. *ACS Catal.* **2018**, *8* (12), 10938−10948.
(110) Kempler, P. A.; Gonzalez, M. A.; Papadantonakis, K. M.; Lewis, N. S. Hydrogen Evolution with Minimal Parasitic Light Absorption by Dense Co-P Catalyst Films on Structured p-Si Photocathodes. *ACS Energy Lett.* **2018**, *3* (3), 612−617.
(111) Yalamanchili, S.; Verlage, E.; Cheng, W. H.; Fountaine, K. T.; Jahelka, P. R.; Kempler, P. A.; Saive, R.; Lewis, N. S.; Atwater, H. A. High Broadband Light Transmission for Solar Fuels Production Using Dielectric Optical Waveguides in TiO_2 Nanocone Arrays. *Nano Lett.* **2020**, *20* (1), 502−508.
(112) Kempler, P. A.; Richter, M. H.; Cheng, W. H.; Brunschwig, B. S.; Lewis, N. S. Si Microwire-Array Photocathodes Decorated with Cu Allow CO_2 Reduction with Minimal Parasitic Absorption of Sunlight. *ACS Energy Lett.* **2020**, *5* (8), 2528−2534.
(113) Ghobadi, A.; Ulusoy Ghobadi, T. G.; Karadas, F.; Ozbay, E. Semiconductor Thin Film Based Metasurfaces and Metamaterials for Photovoltaic and Photoelectrochemical Water Splitting Applications. *Adv. Opt. Mater.* **2019**, *7* (14), 1900028.
(114) Qiu, W.; Xiao, S.; Tong, Y.; Yang, S. Toward Efficient Charge Collection and Light Absorption: A Perspective of Light Trapping for Advanced Photoelectrodes. *J. Phys. Chem. C* **2019**, *123* (31), 18753−18770.
(115) Shi, X.; Ueno, K.; Oshikiri, T.; Sun, Q.; Sasaki, K.; Misawa, H. Enhanced Water Splitting under Modal Strong Coupling Conditions. *Nat. Nanotechnol.* **2018**, *13* (10), 953−958.
(116) Choi, K.; Kim, K.; Moon, I. K.; Bang, J.; Oh, J. Subwavelength Photocathodes via Metal-Assisted Chemical Etching of GaAs for Solar Hydrogen Generation. *Nanoscale* **2019**, *11* (32), 15367−15373.
(117) May, M. M.; Lackner, D.; Ohlmann, J.; Dimroth, F.; Van De Krol, R.; Hannappel, T.; Schwarzburg, K. On the Benchmarking of Multi-Junction Photoelectrochemical Fuel Generating Devices. *Sustain. Energy Fuels* **2017**, *1* (3), 492−503.
(118) Bayon, A.; de la Calle, A.; Ghose, K. K.; Page, A.; McNaughton, R. Experimental, Computational and Thermodynamic Studies in Perovskites Metal Oxides for Thermochemical Fuel Production: A Review. *Int. J. Hydrogen Energy* **2020**, *45* (23), 12653−12679.
(119) Bulfin, B.; Vieten, J.; Agrafiotis, C.; Roeb, M.; Sattler, C. Applications and Limitations of Two Step Metal Oxide Thermochemical Redox Cycles; A Review. *J. Mater. Chem. A* **2017**, *5* (36), 18951−18966.
(120) Lange, M.; Roeb, M.; Sattler, C.; Pitz-Paal, R. Entropy Analysis of Solar Two-Step Thermochemical Cycles for Water and Carbon Dioxide Splitting. *Entropy* **2016**, *18* (1), 24.
(121) Li, S.; Wheeler, V. M.; Kreider, P. B.; Lipiński, W. Thermodynamic Analyses of Fuel Production via Solar-Driven Non-Stoichiometric Metal Oxide Redox Cycling. Part 1. Revisiting Flow and Equilibrium Assumptions. *Energy Fuels* **2018**, *32* (10), 10838−10847.
(122) Kong, H.; Kong, X.; Wang, H.; Wang, J. A Strategy for Optimizing Efficiencies of Solar Thermochemical Fuel Production Based on Nonstoichiometric Oxides. *Int. J. Hydrogen Energy* **2019**, *44* (36), 19585−19594.
(123) Hathaway, B. J.; Chandran, R. B.; Gladen, A. C.; Chase, T. R.; Davidson, J. H. Demonstration of a Solar Reactor for Carbon Dioxide Splitting via the Isothermal Ceria Redox Cycle and Practical Implications. *Energy Fuels* **2016**, *30* (8), 6654−6661.
(124) Hathaway, B. J.; Bala Chandran, R.; Sedler, S.; Thomas, D.; Gladen, A.; Chase, T.; Davidson, J. H. Effect of Flow Rates on Operation of a Solar Thermochemical Reactor for Splitting CO_2 Via the Isothermal Ceria Redox Cycle. *J. Sol. Energy Eng.* **2016**, *138* (1). DOI: 10.1115/1.4032019.
(125) Banerjee, A.; Chandran, R. B.; Davidson, J. H. Experimental Investigation of a Reticulated Porous Alumina Heat Exchanger for High Temperature Gas Heat Recovery. *Appl. Therm. Eng.* **2015**, *75*, 889−895.
(126) Bala Chandran, R.; De Smith, R. M.; Davidson, J. H. Model of an Integrated Solar Thermochemical Reactor/Reticulated Ceramic Foam Heat Exchanger for Gas-Phase Heat Recovery. *Int. J. Heat Mass Transfer* **2015**, *81*, 404−414.
(127) Kumaravel, V.; Bartlett, J.; Pillai, S. C. Photoelectrochemical Conversion of Carbon Dioxide (CO_2) into Fuels and Value-Added Products. *ACS Energy Lett.* **2020**, *5*, 486−519.
(128) Li, C.; Wang, T.; Zhao, Z.-J.; Yang, W.; Li, J.-F.; Li, A.; Yang, Z.; Ozin, G. A.; Gong, J. Promoted Fixation of Molecular Nitrogen with Surface Oxygen Vacancies on Plasmon-Enhanced TiO2 Photoelectrodes. *Angew. Chem., Int. Ed.* **2018**, *57* (19), 5278−5282.
(129) Song, J. T.; Song, H.; Kim, B.; Oh, J. Towards Higher Rate Electrochemical CO_2 Conversion: From Liquid-Phase to Gas-Phase Systems. *Catalysts* **2019**, *9* (3), 224.
(130) Lazouski, N.; Chung, M.; Williams, K.; Gala, M. L.; Manthiram, K. Non-Aqueous Gas Diffusion Electrodes for Rapid Ammonia Synthesis from Nitrogen and Water-Splitting-Derived Hydrogen. *Nat. Catal.* **2020**, *3* (5), 463−469.
(131) Greenblatt, J. B.; Miller, D. J.; Ager, J. W.; Houle, F. A.; Sharp, I. D. The Technical and Energetic Challenges of Separating (Photo)Electrochemical Carbon Dioxide Reduction Products. *Joule* **2018**, *2* (3), 381−420.
(132) Farr, T. P.; Nguyen, N. P.; Bush, H. E.; Ambrosini, A.; Loutzenhiser, P. G. An A- and B-Site Substitutional Study of $SrFeO_3$-δ Perovskites for Solar Thermochemical Air Separation. *Materials* **2020**, *13* (22), 5123.
(133) Michalsky, R.; Parman, B. J.; Amanor-Boadu, V.; Pfromm, P. H. Solar Thermochemical Production of Ammonia from Water, Air and Sunlight: Thermodynamic and Economic Analyses. *Energy* **2012**, *42* (1), 251−260.